Geochemistry Geophysics Geosystems G3

Article
Volume 12, Number 5
11 May 2011
Q0AC11, doi:10.1029/2010GC003482
ISSN: 1525-2027

Published by AGU and the Geochemical Society

# Insights into mantle composition and mantle melting beneath mid-ocean ridges from postspreading volcanism on the fossil Galapagos Rise

**Karsten M. Haase**
*GeoZentrum Nordbayern, Universität Erlangen-Nürnberg, Schlossgarten 5, D-91054 Erlangen, Germany (Karsten.Haase@geol.uni-erlangen.de)*

*Previously at Institut für Geowissenschaften der Universität Kiel, Olshausenstrasse 40, D-24118 Kiel, Germany*

**Marcel Regelous**
*GeoZentrum Nordbayern, Universität Erlangen-Nürnberg, Schlossgarten 5, D-91054 Erlangen, Germany*

**Robert A. Duncan**
*College of Oceanic and Atmospheric Sciences, Oregon State University, Corvallis, Oregon 97331-5503, USA*

**Philipp A. Brandl**
*GeoZentrum Nordbayern, Universität Erlangen-Nürnberg, Schlossgarten 5, D-91054 Erlangen, Germany*

**Nicole Stroncik**
*GeoForschungsZentrum Potsdam, Telegrafenberg B123, D-14473 Potsdam, Germany*

**Ingo Grevemeyer**
*Leibniz-Institut für Meereswissenschaften an der Universität Kiel, Wischofstrasse 1-3, D-24148 Kiel, Germany*

[1] New major and trace element and Sr, Nd, and Pb isotope data, together with $^{39}Ar$-$^{40}Ar$ ages for lavas from the extinct Galapagos Rise spreading center in the eastern Pacific reveal the evolution in magma compositions erupted during slowdown and after the end of active spreading at a mid-ocean ridge. Lavas erupted at 9.2 Ma, immediately prior to the end of spreading are incompatible element depleted mid-ocean ridge tholeiitic basalts, whereas progressively younger (7.5 to 5.7 Ma) postspreading lavas are increasingly alkalic, have higher concentrations of incompatible elements, higher La/Yb, K/Ti, $^{87}Sr/^{86}Sr$, and lower $^{143}Nd/^{144}Nd$ ratios and were produced by smaller degrees of mantle melting. The large, correlated variations in trace element and isotope compositions can only be explained by melting of heterogenous mantle, in which incompatible trace element enriched lithologies preferentially contribute to smaller degree mantle melts. The effects of variable degrees of melting of heterogeneous mantle on lava compositions must be taken into account when using mid-ocean ridge basalt (MORB) to infer the conditions of melting beneath active spreading ridges. For example, the stronger "garnet signature" inferred from Sm/Nd and $^{143}Nd/^{144}Nd$ ratios for postspreading lavas from the Galapagos Rise results from a larger contribution from enriched lithologies with high La/Yb and Sm/Yb, rather than from a greater proportion of melting in the stability field of garnet peridotite. Correlations between ridge depth and Sm/Yb and fractionation-corrected Na concentrations in MORB worldwide could result from variations in mantle fertility and/or variations in

the average degree of melting, rather than from large variations in mantle temperature. If more fertile mantle lithologies are preferentially melted beneath active spreading ridges, then the upper mantle may be significantly more "depleted" than is generally inferred from the compositions of MORB.

**Components:** 14,200 words, 8 figures, 2 tables.

**Keywords:** magmatism; geochemistry; radiogenic isotope.

**Index Terms:** 1032 Geochemistry: Mid-oceanic ridge processes (3614, 8416); 1037 Geochemistry: Magma genesis and partial melting (3619); 1065 Geochemistry: Major and trace element geochemistry.

**Received** 10 January 2011; **Revised** 8 March 2011; **Accepted** 17 March 2011; **Published** 11 May 2011.

Haase, K. M., M. Regelous, R. A. Duncan, P. A. Brandl, N. Stroncik, and I. Grevemeyer (2011), Insights into mantle composition and mantle melting beneath mid-ocean ridges from postspreading volcanism on the fossil Galapagos Rise, *Geochem. Geophys. Geosyst.*, *12*, Q0AC11, doi:10.1029/2010GC003482.

**Theme:** Geochemical Heterogeneities in Oceanic Island Basalt and Mid-ocean Ridge Basalt Sources: Implications for Melting Processes and Mantle Dynamics
**Guest Editors:** C. Beier and P. Asimow

## 1. Introduction

[2] Numerous studies of the lavas erupted at active mid-ocean spreading ridges have shown that even in the absence of nearby hot spots, the upper mantle is chemically and isotopically heterogeneous. At most spreading ridges, a spectrum of lava compositions is observed, ranging from highly depleted lavas (NMORB) with low $^{87}Sr/^{86}Sr$, high $^{143}Nd/^{144}Nd$, low concentrations of incompatible elements, and lower ratios of more to less incompatible elements (e.g., La/Sm), to rarer, highly enriched mid-ocean ridge basalt (EMORB) with high concentrations of incompatible elements, high $^{87}Sr/^{86}Sr$ and low $^{143}Nd/^{144}Nd$. The enriched isotopic characteristics of EMORB indicates that these heterogeneities may have "ages" of a few hundred Myr [e.g., *Donnelly et al.*, 2004]. The origin of these heterogeneities is debated, but they may have an origin in recycled material that was metasomatised by small degree melts, either in the lowermost oceanic lithosphere close to spreading ridges, or in the mantle overlying the slab at subduction zones [*Niu et al.*, 2002; *Donnelly et al.*, 2004; *Pilet et al.*, 2005]. The distribution of compositions is skewed, such that the more enriched EMORB make up a smaller proportion of the lavas erupted at most ridges, and the log distribution of concentrations of highly incompatible elements such as Th is approximately normal [*Arevalo and McDonough*, 2010]. The enriched material apparently makes up a small volume of the upper mantle, possibly in the form of "veins" or streaks, but may contain significantly higher concentrations of the most incompatible elements compared to the enclosing depleted matrix [*Batiza and Vanko*, 1984; *Sleep*, 1984; *Zindler et al.*, 1984; *Prinzhofer et al.*, 1989].

[3] Several lines of evidence suggest that enriched mantle lithologies may have lower solidus temperature than the more depleted matrix, and so are preferentially tapped at low degrees of melting [*Sleep*, 1984; *Prinzhofer et al.*, 1989; *Ito and Mahoney*, 2005a]. Lavas erupted at intratransform spreading segments in the Garrett Fracture Zone, interpreted to result from melting of mantle that recently underwent melt extraction beneath the adjacent spreading ridge, have trace element and isotope compositions that are more depleted than lavas from neighboring ridge segments [*Wendt et al.*, 1999]. Conversely, lavas believed to result from small degrees of mantle melting tend to have more enriched incompatible trace element and isotope compositions [e.g., *Haase*, 1996; *Janney et al.*, 2000; *Regelous et al.*, 2003; *Hirano et al.*, 2006; *Konter et al.*, 2009; *Castillo et al.*, 2010]. Clinopyroxenes in residual abyssal peridotites tend to have more radiogenic Nd isotope compositions than those of lavas from the same section of ridge, consistent with preferential melting-out of eclogite or pyroxenite with lower Sm/Nd and $^{143}Nd/^{144}Nd$ ratios during decompression melting [*Salters and Dick*, 2002]. Although these observations could be explained by melting of heterogeneous mantle in which enriched lithologies melt to a greater extent than more depleted lithologies, such "nonmodal" melting has not been convincingly demonstrated. Yet if this process is important during mantle melting beneath

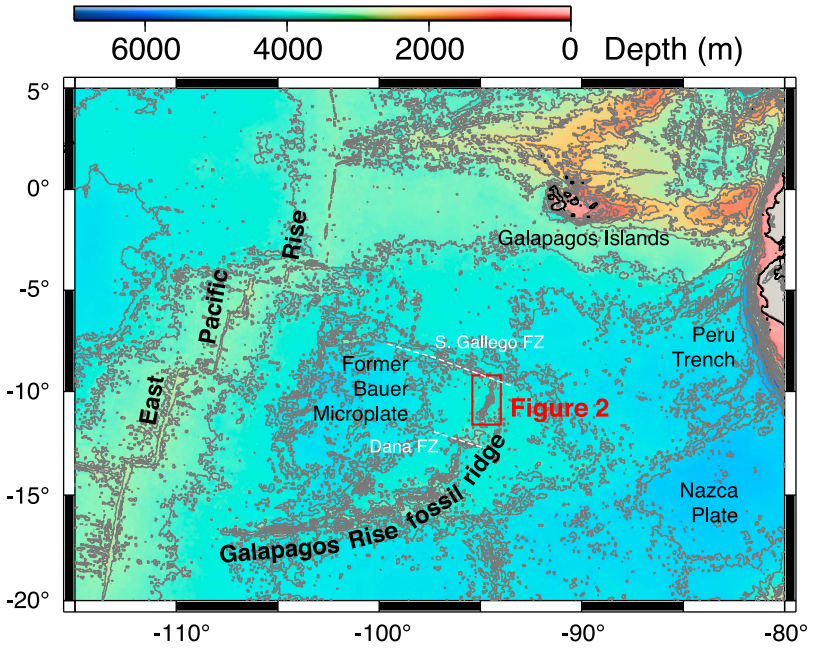


**Figure 1.** Tectonic map of the eastern Pacific, showing the location of the Galapagos Rise fossil spreading center on the Nazca Plate to the east of the active East Pacific Rise. The three fossil ridge segments immediately south of the South Gallego Fracture Zone (red box) were sampled during R/V *Sonne* cruise SO-160 (see Figure 2).

spreading ridges, then melting models that assume that the mantle is homogenous at the scale of the melting region [e.g., *Klein and Langmuir*, 1987; *Salters and Hart*, 1989; *McKenzie and O'Nions*, 1991; *Spiegelman and Elliott*, 1993] are unlikely to be realistic.

[4] Fossil spreading ridges, formed when active spreading centers are abandoned, may continue to erupt magma for several million years after plate separation has ceased [*Batiza*, 1977; *Batiza et al.*, 1982; *Batiza and Vanko*, 1985; *Davis et al.*, 2002; *Clague et al.*, 2009; *Haase et al.*, 2011]. Previous geochemical studies of the youngest lavas erupted at fossil spreading ridges have shown that many are EMORB, with highly enriched trace element and isotope compositions [*Batiza and Vanko*, 1985; *Bohrson and Reid*, 1995; *Choe et al.*, 2007; *Choi et al.*, 2008; *Clague et al.*, 2009; *Castillo et al.*, 2010; *Haase et al.*, 2011; *Tian et al.*, 2011]. Postspreading lavas erupted at fossil ridges may therefore preserve the purest expression of the EMORB source among all oceanic basalts away from hot spots, and they apparently result from smaller degrees of mantle melting of the same "normal" mantle that melts beneath actively spreading ridges to produce MORB. The compositions of postspreading lavas may therefore give unique insights into the effects of mantle heterogeneity and the degree of mantle melting on the compositions of melts erupted at spreading ridges [*Batiza*, 1989; *Castillo et al.*, 2010]. On many fossil ridges, the compositions of these postspreading lavas vary systematically with age at a given location [e.g., *Castillo et al.*, 2010; *Haase et al.*, 2011], and may therefore potentially be used to infer changes in the degree and depth of melting during slowdown and eventual cessation of spreading.

[5] We present here new major and trace element and Sr, Nd, Pb isotope data, and $^{39}$Ar-$^{40}$Ar ages for lavas erupted during the late spreading and postspreading stages of the extinct Galapagos Rise spreading center.

## 2. Tectonic Setting and Sample Locations

[6] The Galapagos Rise is an extinct (fossil) spreading center located on the Nazca Plate in the southeastern Pacific [*Menard et al.*, 1964]. Spreading at this ridge, between the Nazca Plate to the east and the Bauer Microplate to the west, began 18.5 Ma ago, but was abandoned approximately 12 Myr later when spreading was transferred to the East Pacific Rise, 900 km to the west (Figure 1). Until spreading ceased, the Galapagos Rise at 10°S was a fast spreading ridge with an average spreading rate of 170 mm/yr. Spreading is estimated to have slowed

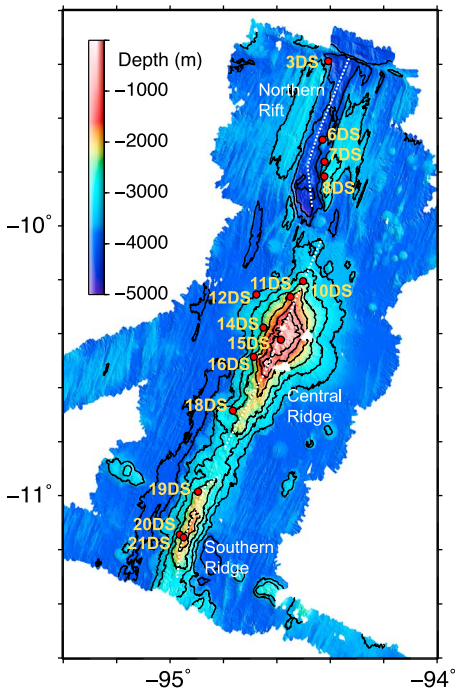


**Figure 2.** Bathymetric map of the Galapagos Rise fossil spreading axis between 9°20′ S and 11°20′ S, showing locations of dredged samples (red circles). Bathymetric contours are in 500 m intervals. A deep (>4000 m) axial rift characterizes the southern end of the northernmost segment (the Northern Rift), whereas an axial ridge is present on the two southern segments (Central and Southern ridges). The volcanic ridges show no evidence of tectonic disturbance and were therefore constructed after spreading had ceased, by lavas that filled the axial rift and constructed elongated seamounts that rise up to 2500 m above the surrounding seafloor to within 500 of sea level. The three samples dated in this study are from dredges 3DS, 14DS, and 19DS.

dramatically at about 6.5 Ma, and the ridge was finally abandoned at the time of Bauer Microplate capture by the Nazca Plate at 5.8 Ma, based on bathymetric and magnetic data [*Anderson and Sclater*, 1972; *Herron*, 1972; *Mammerickx et al.*, 1980; *Eakins and Lonsdale*, 2003].

[7] During R/V *Sonne* cruise SO-160, a detailed bathymetric survey and sample dredging program was carried out along three ridge segments of the Galapagos Rise, each approximately 50 km in length, between the Dana Fracture Zone to the south and the South Gallego FZ to the north [*Haase et al.*, 2002]. The southern end of the northernmost segment is characterized by an axial rift, up to 4700 m deep, with a sigmoidal shape (Figure 2). A characteristic nodal deep and an inside corner high occur at the former ridge-transform intersection at the southern end of this segment (Figure 2). This type of ridge-transform morphology is typical of slow spreading ridges and is rarely observed at fast spreading ridges, confirming that the spreading rate on the Galapagos Rise slowed dramatically prior to extinction. A similar change in ridge morphology occurred shortly before the abandonment of the Mathematician Ridge [*Batiza and Vanko*, 1985].

[8] South of the transform offset at approximately 10°S, the Galapagos Rise has a very different morphology. No axial rift is observed, instead an axial ridge is present, which at its northern end rises about 2500 m above the surrounding seafloor to within 500 m of sea level (Figure 2). The ridge is capped by volcanic cones with heights of several hundred meters; similar cones occur on the flanks of the ridge and on the surrounding seafloor, and these are likely the youngest volcanic features of this ridge segment [*Haase et al.*, 2002]. A second, less pronounced axial high is present immediately to the south of a small offset of the ridge at 10°55′S (Figure 2). The lack of tectonic disturbance of these younger ridge-centered volcanic features indicates that extension at the ridge axis had ceased at the time of their formation. Similar large, postspreading central volcanoes, elongated parallel to the former spreading axis and partially covering older structures have been reported from the Mathematician and Guadelupe fossil ridges in the North Pacific and the extinct Wharton Ridge in the northern Indian Ocean. Some volcanoes built on fossil ridges may become emergent (for example Guadalupe and Socorro Islands), but there is no evidence from either volcano morphology or the petrology of dredged samples that the summit of the large seamount on the Galapagos Rise at 10°24′ S was previously above sea level.

## 3. Samples and Analytical Methods

[9] During cruise SO-160, samples of volcanic rock were recovered by dredging from four locations along the deep axial rift in the northern part of the study area, and ten locations along the shallow axial volcanic ridge to the south (Figure 2). A total of 42 of the freshest samples (13 from the axial rift, 29 from the axial ridge) were selected for analysis. Most lavas dredged from the rift are plagioclase, plagioclase ± clinopyroxene, or plagioclase ± olivine phyric, sparsely vesicular basalts, those dredged from the axial ridge and its flanks are mainly aphyric or sparsely plagioclase phyric, vesicular basalts. Fresh volcanic glass was present on many samples, and as far as possible, analyses were carried out on hand-

picked glasses. Weathered surfaces were removed from whole-rock samples, which were then coarse crushed, washed thoroughly in deionized water, and powdered in an agate mortar.

[10] Major and trace element analyses were carried out at the Institut für Geowissenschaften at the Universität Kiel. For whole-rock major element analysis, 0.6 g of dried rock powder was mixed with lithium tetraborate and ammonium nitrate, fused to a homogenous glass bead, and analyzed using a Phillips PW1400 XRF spectrometer calibrated against international rock standards. Magnesium numbers ($Mg\# = 100 \times Mg^{2+}/(Mg^{2+} + Fe^{2+})$) were calculated assuming $FeO = 0.86 \times FeO_{TOTAL}$. Major element compositions of glasses were determined by electron microprobe (JEOL 8900 Superprobe). For glass analyses, a 12$\mu$m defocused beam at 15nA beam current and 15kV acceleration was used. The instrument was calibrated against natural glass standards, and precision and accuracy for the VG-2 standard were better than 1% for all major elements. Trace element concentrations of both glass and whole-rock samples were determined using an upgraded PlasmaQuad ICP-MS following the procedure outlined by *Garbe-Schönberg* [1993]. Glass samples were washed in ultrapure water in an ultrasonic bath before analysis. Accuracy was checked using international rock standards (data for BHVO-1 are given for reference in Table 1), and the external precision for most elements was better than 5%.

[11] Before dissolution for isotope measurements, rock powders were leached for 1 h in hot, ultrapure 6M HCl, then washed thoroughly with ultrapure water. Glass samples were washed but not leached before dissolution. Ion exchange techniques used for Sr, Nd and Pb separation are described by *Hoernle and Tilton* [1991]. Sr and Pb isotope measurements were carried out at the GEOMAR Kiel, using a Finnigan MAT 262 thermal ionization mass spectrometer in static mode. Nd isotope ratios were analyzed in dynamic mode on the same instrument. Fractionation corrections were made assuming $^{86}Sr/^{88}Sr = 0.1194$ and $^{146}Nd/^{144}Nd = 0.7219$. Repeat measurements of NBS987 yielded $^{87}Sr/^{86}Sr = 0.710218 \pm 0.000024$ ($2\sigma$, n = 12). Repeat measurements of the Spex and La Jolla Nd standards gave $^{143}Nd/^{144}Nd$ values of 0.511710 (n = 15) and $0.511827 \pm 0.000007$ ($2\sigma$, n = 3), respectively. Data in Table 1 are normalized to values of 0.710250 and 0.511855 for the NBS987 and La Jolla standards. Pb isotope measurements were fractionation corrected using repeat measurements of NBS981 ($^{206}Pb/^{204}Pb$ 16.909 ± 0.017, $^{207}Pb/^{204}Pb$ 15.455 ± 0.022, $^{208}Pb/^{204}Pb$ 36.584 ± 0.069), and normalized to the values of *Todt et al.* [1996]. Pb blanks were negligible (<50 pg).

[12] Three samples were selected for dating using the $^{40}Ar$-$^{39}Ar$ method. An acid-leached plagioclase separate from sample 14DS-2, and whole-rock portions of samples 3DS-1 and 19DS-1 were irradiated in the 1MW TRIGA reactor at Oregon State University for 6 h together with FCT-3 biotite (28.04 Ma) as flux monitor. Details of the analytical methods used are given by *Koppers et al.* [2003] and *Duncan and Keller* [2004]. Age plateaus and isochron ages (Table 2) were calculated using software described by *Koppers* [2002].

## 4. Results

### 4.1. Ar-Ar Ages of Galapagos Rise Lavas

[13] Sample 3DS-1, from the shoulder of the deep rift at 9°24′ S (hereafter the Northern Rift) yielded an weighted plateau $^{40}Ar$-$^{39}Ar$ age of 9.18 ± 0.44 Ma, which represents a maximum age for the abandonment of spreading, since by analogy with the volcanically active rift zone of the Mid-Atlantic Ridge the last lavas erupted on this ridge segment were likely emplaced within the rift floor. On the basis of bathymetric and magnetic data, spreading at the Galapagos Rise is estimated to have finally ceased at 6.5 Ma [*Anderson and Sclater*, 1972; *Mammerickx et al.*, 1980; *Eakins and Lonsdale*, 2003], which may indicate that lavas within the rift itself span an age range of 2–3 Ma.

[14] The two lavas from the volcanic ridge yielded significantly younger $^{40}Ar$-$^{39}Ar$ ages. Sample 14DS-2, from the western flank of the larger, northern axial high centered at 10°24′ S (Central Ridge) has an age of 5.66 ± 0.88 Ma, whereas sample 19DS-1, which was dredged from the southern, smaller high along the axial ridge near 11°05′ S (Southern Ridge) yielded an age of 7.50 ± 0.60 Ma. There is no evidence that these younger volcanic features have been disrupted by faulting, which suggests that active spreading on this part of the Galapagos Rise ended at between 9.2 and 7.5 Ma. The youngest of the three ages reported here was obtained from the largest volcanic construction, and is probably a maximum age for the youngest flows, since this sample was dredged from the ridge flanks, rather than from the small cones close to the summit region which are likely to be the youngest volcanic features. Based on our new ages,

**Table 1 (Sample).** Geochemical and Isotopic Compositions of the Galapagos Rise Lavas [The full Table 1 is available in the HTML version of this article]

| | Sample Name | | | | | | | | |
|---|---|---|---|---|---|---|---|---|---|
| | SO160 3DS-1 | SO160 3DS-2 | SO160 3DS-6 | SO160 6DS-1 | SO160 3DS-3 | SO160 3DS-4 | SO160 3DS-5 | SO160 8DS-2 | SO160 8DS-3 |
| Location | Northern Rift | Northern Rift | Northern Rift | Northern Rift | Northern Rift | Northern Rift | Northern Rift | Northern Rift | Northern Rift |
| Latitude (°S) | −9.3866 | −9.3866 | −9.3866 | −9.6801 | −9.3866 | −9.3866 | −9.3866 | −9.8170 | −9.8170 |
| Longitude (°W) | 94.4060 | 94.4060 | 94.4060 | 94.4269 | 94.4060 | 94.4060 | 94.4060 | 94.4235 | 94.4235 |
| Depth | 3896 | 3896 | 3896 | 3814 | 3896 | 3896 | 3896 | 2973 | 2973 |
| Sample Type | Glass | Glass | Glass | Glass | Whole rock | Whole rock | Whole rock | Whole rock | Whole rock |
| SiO2 | 51.17 | 50.97 | 51.08 | 51.22 | 51.42 | 51.04 | 50.28 | 51.76 | 50.28 |
| TiO2 | 2.02 | 2.03 | 1.93 | 1.17 | 1.87 | 1.65 | 1.69 | 1.26 | 1.22 |
| Al2O3 | 14.39 | 14.42 | 14.57 | 15.33 | 15.57 | 16.15 | 16.14 | 15.32 | 15.61 |
| Fe2O3 | | | | | 9.08 | 9.25 | 10.25 | 8.79 | 9.39 |
| FeO | 10.97 | 10.89 | 10.16 | 8.51 | | | | | |
| MnO | 0.19 | 0.18 | 0.20 | 0.17 | 0.17 | 0.16 | 0.16 | 0.16 | 0.15 |
| MgO | 6.82 | 6.84 | 7.18 | 8.34 | 6.22 | 6.25 | 6.64 | 7.76 | 8.00 |
| CaO | 11.18 | 11.13 | 11.12 | 12.92 | 11.97 | 12.19 | 11.69 | 12.52 | 12.17 |
| Na2O | 2.93 | 3.00 | 2.59 | 1.99 | 2.76 | 2.77 | 2.58 | 2.54 | 2.47 |
| K2O | 0.12 | 0.12 | 0.11 | 0.29 | 0.38 | 0.29 | 0.26 | 0.21 | 0.13 |
| P2O5 | 0.29 | 0.29 | 0.20 | 0.18 | 0.18 | 0.16 | 0.17 | 0.10 | 0.13 |
| Total | 100.24 | 100.02 | 99.45 | 100.39 | 100.09 | 100.63 | 100.17 | 100.58 | 100.40 |
| Li | 7.22 | 7.53 | | 4.68 | 2.55 | | | | 5.22 |
| Sc | 37.4 | 37.6 | | 43.1 | 30.8 | | | | 37.1 |
| V | 352 | 353 | | 279 | 237 | | | | 277 |
| Cr | 209 | 215 | | 358 | 222 | | | | 286 |
| Co | 38.8 | 39.1 | | 43.1 | 39.6 | | | | 39.8 |
| Ni | 74.5 | 75.1 | | 122.8 | 72.7 | | | | 106.0 |
| Cu | 58.5 | 56.7 | | 85.2 | 49.3 | | | | 69.8 |
| Zn | 87.0 | 86.2 | | 64.0 | 80.6 | | | | 65.3 |
| Rb | 1.72 | 1.54 | | 4.34 | 4.70 | | | | 1.56 |
| Sr | 110 | 111 | | 125 | 148 | | | | 129 |
| Y | 41.8 | 41.6 | | 23.9 | 41.0 | | | | 26.7 |
| Zr | 132 | 131 | | 72 | 120 | | | | 75 |
| Nb | 2.48 | 2.44 | | 6.99 | 2.51 | | | | 1.26 |
| Mo | 0.347 | 0.287 | | 0.655 | 0.317 | | | | 0.301 |
| Sn | 1.29 | 1.30 | | 0.62 | 1.33 | | | | 0.92 |
| Sb | 0.025 | 0.013 | | 0.033 | 0.026 | | | | 0.010 |
| Cs | 0.027 | 0.020 | | 0.041 | 0.141 | | | | 0.035 |
| Ba | 15.70 | 14.60 | | 54.46 | 40.13 | | | | 6.73 |
| La | 4.14 | 4.10 | | 5.52 | 4.36 | | | | 2.38 |
| Ce | 13.40 | 13.30 | | 13.21 | 14.01 | | | | 7.99 |
| Pr | 2.42 | 2.40 | | 1.93 | 2.52 | | | | 1.41 |
| Nd | 13.40 | 13.30 | | 8.62 | 13.73 | | | | 7.80 |
| Sm | 4.77 | 4.73 | | 2.61 | 4.92 | | | | 2.87 |
| Eu | 1.61 | 1.61 | | 0.95 | 1.65 | | | | 1.06 |

**Table 2.** Summary of $^{40}Ar$-$^{39}Ar$ Data for Lavas from the Galapagos Rise Fossil Spreading Center[a]

| Sample | Code | Sample Type | Weighted Plateau | | | | Total Fusion | Inverse Isochron | |
|---|---|---|---|---|---|---|---|---|---|
| | | | Age (Ma) | N | % $^{39}Ar$ | MSWD | Age (Ma) | Age (Ma) | $^{40}Ar/^{36}Ar$ |
| 3DS-1 | 02C9947 | Whole rock | 9.18 ± 0.44 | 7 | 100 | 1.10 | 9.43 ± 0.75 | 6.70 ± 3.14 | 303.5 ± 11.9 |
| 14DS-2 | 02C2931 | Plagioclase | 5.66 ± 0.88 | 6 | 99.3 | 0.33 | 6.20 ± 0.90 | 4.86 ± 1.79 | 300.5 ± 9.7 |
| 19DS-1 | 02C3045 | Whole rock | 7.50 ± 0.60 | 7 | 100 | 0.50 | 8.00 ± 0.85 | 5.63 ± 2.59 | 299.2 ± 5.2 |

[a]N is number of heating steps, and % $^{39}Ar$ indicates percentage of total $^{39}Ar$ released used in plateau age calculation. Total decay constant of $^{40}K$ is taken to be $5.530 \times 10^{10}$ $yr^{-1}$. All errors: 2s.

magmatism on the Galapagos Rise therefore continued along part of its length for at least 1.8 Myr after spreading ceased, with postspreading lava flows filling the rift and building an axial ridge.

## 4.2. Major and Trace Element Geochemistry

[15] New major and trace element data for Galapagos Rise lavas are listed in Table 1. All samples recovered from the Northern Rift are tholeiitic basalts, with MgO concentrations of 6.22 to 8.61%. The 4 glass samples from dredges 3DS and 6DS lie on well-defined lines in major element diagrams, whereas whole-rock samples show more scatter, due to the effects of alteration or variable phenocryst contents (Figure 3). With the exception of one sample (6DS-1), lavas from the Northern Rift have $K_2O/TiO_2$ and La/Sm ratios of 0.06–0.20 and 0.65–0.97, respectively (Figures 3 and 4). Their major and trace element compositions therefore lie within the range of normal depleted mid-ocean ridge basalts, but at the depleted end of this range. For example, Nb concentrations of the most depleted samples are <1 ppm (Figure 4), and the low La/Sm and Nb/Zr ratios in these samples overlap with the most depleted lavas from near-ridge seamounts on the flanks of the East Pacific Rise (Figure 4), which have highly variable trace element compositions [*Niu and Batiza*, 1997]. However, Rb and Ba concentrations are within the range of normal MORB, and thus Ba/Nb and Ba/Th ratios of the lavas from the Northern Rift are relatively high (Figure 4).

[16] Lavas from the Central and Southern ridges are alkalic basalts with lower MgO concentrations than the lavas from the Northern Rift. Highly evolved lavas, such as trachytes and rhyolites which have been reported from some postspreading structures located on other fossil spreading ridges [e.g., *Batiza*, 1977, 1989; *Davis et al.*, 1995] are not among the samples we have analyzed from the Galapagos Rise. However, dredge 15DS from a cone on the summit recovered a fragment of apparently heavily altered trachyte [*Haase et al.*, 2002]. Major element compositions of lavas from the Northern Rift and from the Central and Southern ridges overlap, but for a given MgO, lavas from the latter have lower $SiO_2$, FeO, CaO, higher $Al_2O_3$, $Na_2O$, and significantly higher $K_2O$ (Figure 3). Lavas from the Central and Southern ridges are alkalic basalts with high concentrations of highly incompatible elements, and higher ratios of more to less incompatible elements, e.g., $K_2O/TiO_2$, La/Sm, Nb/Zr, compared to lavas from the Northern Rift (Figures 3 and 4). The most enriched lavas have Th, Nb concentrations and Nb/Zr, La/Sm ratios that overlap with those of the most enriched East Pacific Rise (EPR) seamount lavas and extend to higher values (Figure 4). These lavas therefore include some of the most "enriched" examples of oceanic basalts not associated with long-lived intraplate ("hot spot") magmatism. A very wide range of magma compositions was thus erupted at the Galapagos Rise axis within a 2 to 3 Ma period and over a distance of approximately 150 km; for instance Th and Nb concentrations in Galapagos Rise lavas vary by over 2 orders of magnitude (Figure 4) despite a limited range in MgO and Mg#, and La/Sm and Nb/Zr ratios show a similar range to that found in EPR seamount lavas (Figure 4), which encompass much of the range observed within MORB worldwide [*Niu and Batiza*, 1997].

[17] There is evidence that seafloor alteration and weathering may have affected the concentrations of more mobile elements in whole-rock samples. For example, the glass samples have Nb/U within the range of fresh oceanic basalts (43–47), whereas whole-rock samples have lower and more variable ratios of between 23 and 33. Whole-rock samples also have more variable Ce/Pb (11–26) and Ba/Rb (4.3–35; not shown) than those typical of fresh oceanic basalts (25 ± 5 and 11 ± 3, respectively), and are therefore likely to have gained U, Rb and Pb. Interestingly, both whole-rock and glass samples have relatively high Ba/Th and Ba/Nb ratios compared to most MORB, and so the relatively high Ba concentrations of lavas from the Northern Rift (Figure 3) are therefore apparently a primary feature unrelated to alteration. Nevertheless, in the

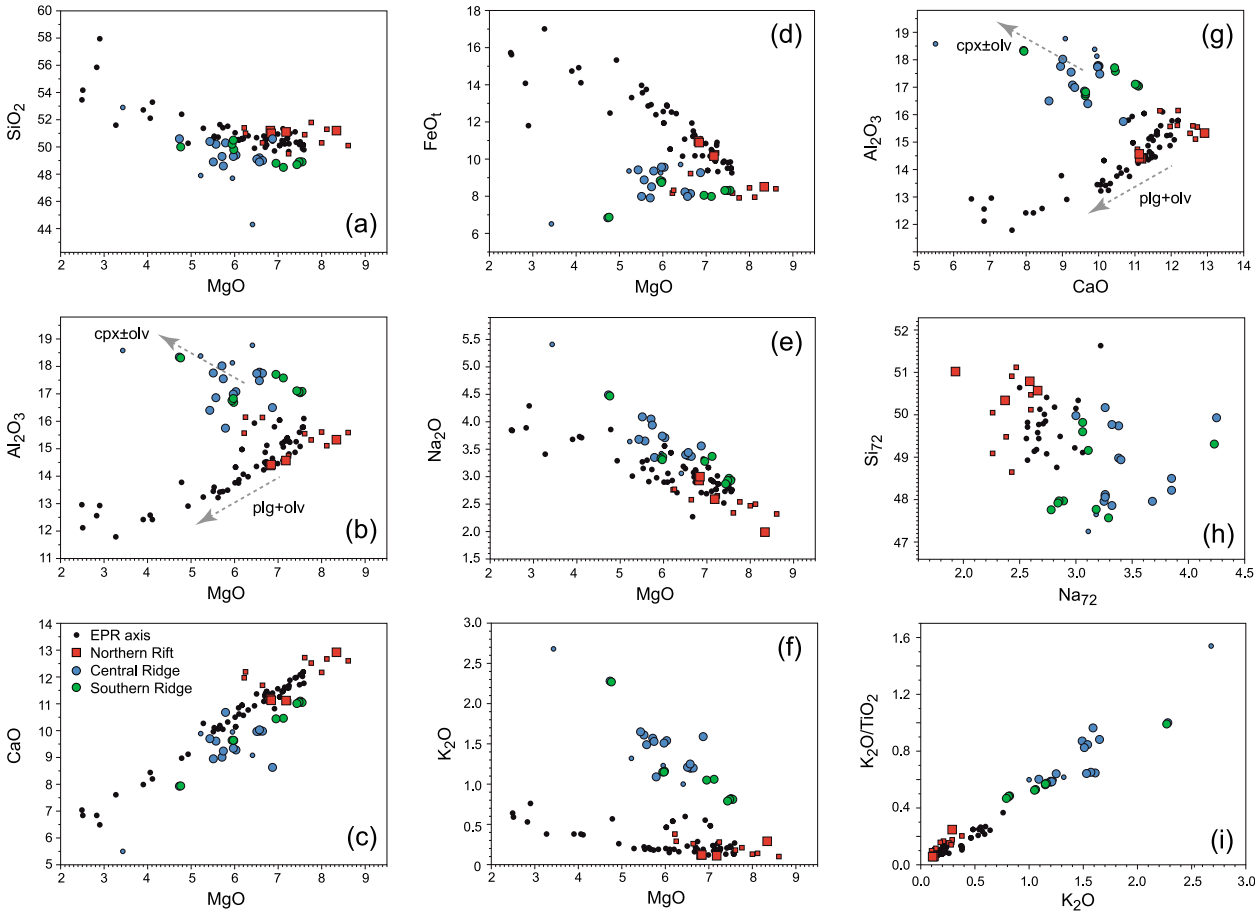


**Figure 3.** Major element compositions of Galapagos Rise lavas. The small symbols are for whole-rock samples, and the large symbols are for glass analyses. Data for basaltic and andesitic lavas from the northern East Pacific Rise (black circles represent data from *Niu et al.* [1999] and *Regelous et al.* [1999]) are shown for comparison. Compared to lavas from the Northern Rift, younger postspreading lavas from the Central and Southern ridges have lower $SiO_2$ and CaO and higher $Na_2O$, $K_2O$, and $Al_2O_3$ for a given MgO. The postspreading lavas also have higher $Na_{72}$ values and extend to lower $Si_{72}$ (where $Na_{72}$ and $Si_{72}$ are $Na_2O$ and $SiO_2$ concentrations corrected for the effects of fractional crystallization to Mg# = 72 using the method of *Niu et al.* [1999]). See the text for discussion.

following discussion we use the less mobile rare earth and high field strength elements to investigate the petrogenesis of the Galapagos Rise lavas.

## 4.3. Sr, Nd, and Pb Isotope Compositions

[18] New Sr, Nd and Pb isotope data for Galapagos Rise lavas are given in Table 1. There are no systematic differences in isotope composition between glasses and leached whole-rock powders, uggesting that any effects of alteration on Sr and Pb isotope compositions have been removed by the leaching rocess. All but one of the samples from the Northern Rift have $^{87}Sr/^{86}Sr$ and $^{143}Nd/^{144}Nd$ ratios of 0.70251–0.70264 and 0.51316–0.51321, respectively, and are distinct from lavas from the Central and Southern ridges (0.70291–0.70311 and 0.51297–0.51303, see Figure 5). One Northern Rift sample (6DS-1) has an intermediate Nd composition, and an $^{87}Sr/^{86}Sr$ ratio that lies within the range of samples from the Southern Ridge. This sample also has the highest La/Sm of the Northern Rift lavas. Lavas from the Central and Southern ridges and from the Northern Rift also have different Pb isotope compositions (Figure 5): the latter have less radiogenic Pb ($^{206}Pb/^{204}Pb$ 17.92–18.09), except for sample 6DS-1 which has a composition within the range of Ridge lavas ($^{206}Pb/^{204}Pb$ 18.50–18.98). Northern Rift lavas have isotope compositions within the range of Pacific MORB far from hot spots, although $^{143}Nd/^{144}Nd$ and $^{206}Pb/^{204}Pb$ ratios lie at the high end and low end of the MORB range, respectively. The Sr and Nd isotope compositions of lavas from the Central and Southern ridges overlap with the enriched (high $^{87}Sr/^{86}Sr$, low

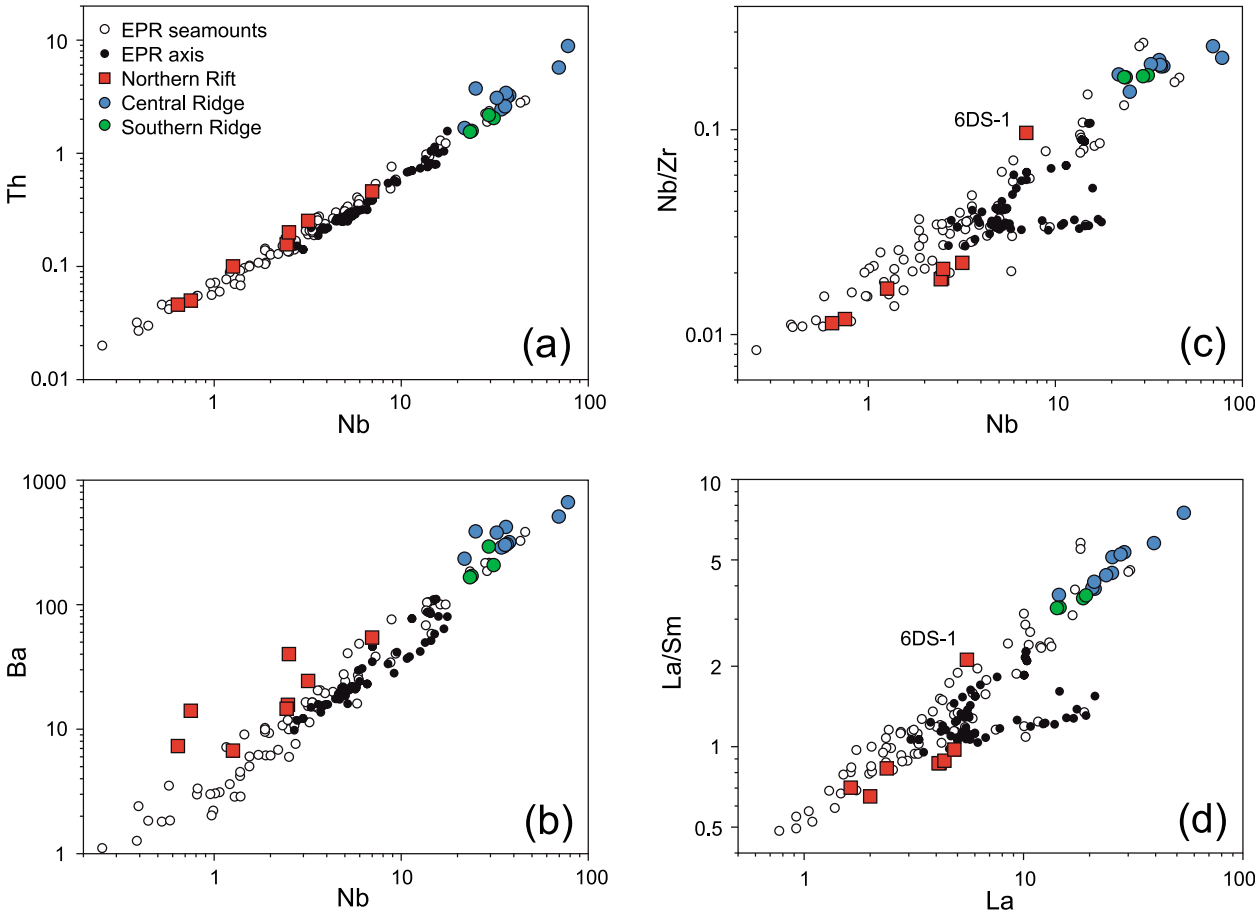


**Figure 4.** Trace element compositions of Galapagos Rise lavas. Variation of (a) Th and (b) Ba with Nb concentrations and (c) Nb/Zr and (d) La/Sm ratios with Nb and La, respectively. Lavas erupted within the Northern Rift during the last stages of active spreading on the Galapagos Rise have low incompatible trace element concentrations and low La/Sm and Nb/Zr ratios that overlap with the range for more depleted lavas from the East Pacific Rise (EPR) and EPR seamounts. In contrast, postspreading lavas from the volcanic ridge have higher concentrations of incompatible trace elements, have high La/Sm and Nb/Zr, and are among the most enriched EMORB found in the ocean basins away from hot spots. Within the postspreading lavas there appears to have been a systematic evolution to more "enriched" compositions between 7.5 Ma (Southern Ridge) to 5.7 Ma (Central Ridge). A very wide range of lava compositions were therefore erupted on the Galapagos Rise within an approximately 2 Ma period. Data for northern EPR MORB and near-ridge seamount lavas are from *Niu and Batiza* [1997], *Niu et al.* [1999, 2002], and *Regelous et al.* [1999].

$^{143}Nd/^{144}Nd$) end of the array defined by Pacific near-ridge seamounts (Figure 5). Lavas from the Galapagos Rise thus display the entire range in Sr and Nd isotope composition observed on eastern Pacific spreading centers and near-ridge seamounts away from hot spots.

[19] Our new $^{40}Ar$-$^{39}Ar$ ages suggest that on the Galapagos Rise there was a systematic evolution of magmatism from incompatible element depleted, NMORB-type tholeiitic basalts toward more alkalic, incompatible element enriched lavas with higher $^{87}Sr/^{86}Sr$ and lower $^{143}Nd/^{144}Nd$ after spreading ceased. Although our geochronological data are limited, a similar temporal evolution in lava compositions has also been reported from the fossil Phoenix Ridge [*Choe et al.*, 2007; *Choi et al.*, 2008; *Haase et al.*, 2011], and fossil spreading centers off Baja California Sur [*Tian et al.*, 2011]. On the Galapagos Rise, the postspreading lavas with the highest $^{87}Sr/^{86}Sr$, $^{206}Pb/^{204}Pb$ and lowest $^{143}Nd/^{144}Nd$ also have the highest incompatible trace element concentrations, and the highest Nb/Zr, La/Sm and $K_2O/TiO_2$ ratios (Figure 6).

## 4.4. Comparison With Lavas From Other Extinct Spreading Centers

[20] Geochemical data for lavas from other fossil spreading centers have been reported from the Math-

ematician, Guadalupe and other extinct ridges in the NE Pacific, including associated subaerial islands [*Batiza and Chase*, 1981; *Batiza and Vanko*, 1985; *Clague et al.*, 2009; *Castillo et al.*, 2010; *Tian et al.*, 2011], the Antarctic-Phoenix Ridge in the Drake Passage [*Choe et al.*, 2007, *Choi et al.*, 2008; *Haase et al.*, 2011], the Wharton Ridge in the northern Indian Ocean [*Hébert et al.*, 1999], as well as the Galapagos Rise [*Batiza et al.*, 1982]. In many cases, the samples analyzed are from volcanic features which were clearly built after spreading ceased.

[21] Based on these previous studies and our new data for the Galapagos Rise, lavas erupted at extinct spreading centers have the following geochemical characteristics: they are generally more alkaline in composition compared to the tholeiites erupted at active spreading centers, and may include relatively evolved lavas such as trachyandesites and trachytes. The latter difference likely results from the lower magma supply rates beneath fossil spreading ridges (compared to active spreading centers) resulting in longer crustal residence times and greater degrees of fractionation. Postspreading lavas from fossil ridges tend to have higher concentrations of incompatible trace elements, and higher ratios of more to less incompatible elements (La/Sm, Nb/Zr, $K_2O/TiO_2$); and generally more radiogenic Sr and less radiogenic Nd isotope compositions (Figure 7). Postspreading magmatism on the Phoenix Ridge, like that on the Galapagos Rise, became increasingly enriched with time [*Haase et al.*, 2011]. To some extent, the major and trace element characteristics of postspreading lavas could result from smaller average degrees of melting, resulting from less extensive mantle upwelling after spreading ceased. However, the isotopic differences also indicate a role for source heterogeneity, as discussed below.

# 5. Discussion

## 5.1. Origin of Chemical and Isotopic Variations

### 5.1.1. Effects of Fractional Crystallization and Melting Processes

[22] There is evidence that lavas from the Northern Rift and from the Central and Southern Ridges have undergone fractionational crystallization of different mineral assemblages, and these differences must be taken into account before attempting to compare differences in mantle source composition and melting conditions between the two lava suites.

[23] Major element compositions of the Northern Rift lavas lie within the range of EPR MORB, and the major element variations are consistent with low-pressure fractionation of olivine + plagioclase ± clinopyroxene. Both CaO and $Al_2O_3$ decrease with decreasing MgO (the relatively high $Al_2O_3$ for a given MgO in 3 samples from dredge 3DS is likely due to plagioclase accumulation in these whole-rock samples). In contrast, within Central and Southern Ridge lavas, $Al_2O_3$ contents are much higher for a given MgO, and do not vary systematically with MgO (Figure 3), indicating that plagioclase fractionation was much less significant. Within these lavas, CaO correlates negatively with $Al_2O_3$ (Figure 3) and Sc correlates positively with MgO, consistent with a role for clinopyroxene ± olivine fractionation in the lavas from the Central and Southern Ridges. Both minerals are common phenocryst phases in these lavas. However, the scatter in major element composition indicates that the lavas cannot be related by crystallization along a single liquid line of descent from a common parental magma.

[24] The difference in fractionation behavior between magmas from the Central and Southern ridges and from the Northern Rift likely reflects a higher pressure of fractionation for the former. At higher pressures, the onset of clinopyroxene crystallization occurs at higher temperature [*Presnall et al.*, 1979; *Tormey et al.*, 1987], resulting in a decrease in CaO and $CaO/Al_2O_3$ with decreasing MgO in residual melts, and relatively high $Al_2O_3$ for a given MgO [e.g., *Eason and Sinton*, 2006]. On a global scale, average pressures of MORB crystallization are negatively correlated with ridge spreading rate [*Michael and Cornell*, 1998], and high-$Al_2O_3$ MORB which are inferred to have undergone extensive clinopyroxene fractionation occur preferentially at ridge segment terminations and dying ridge segments, where high-pressure crystal fractionation is enhanced due to greater conductive cooling and lower magma supply [*Michael and Cornell*, 1998; *Eason and Sinton*, 2006].

[25] Most lavas from the Northern Ridge have lower $Na_2O$ and higher $SiO_2$ for a given MgO compared to lavas from the Central and Southern ridges (Figure 3). The subparallel MgO-$SiO_2$ and MgO-$Na_2O$ arrays defined by synspreading and postspreading lavas indicate that these differences do not result from the differences in fractionation behavior discussed above. The $Na_2O$ and $SiO_2$ concentrations

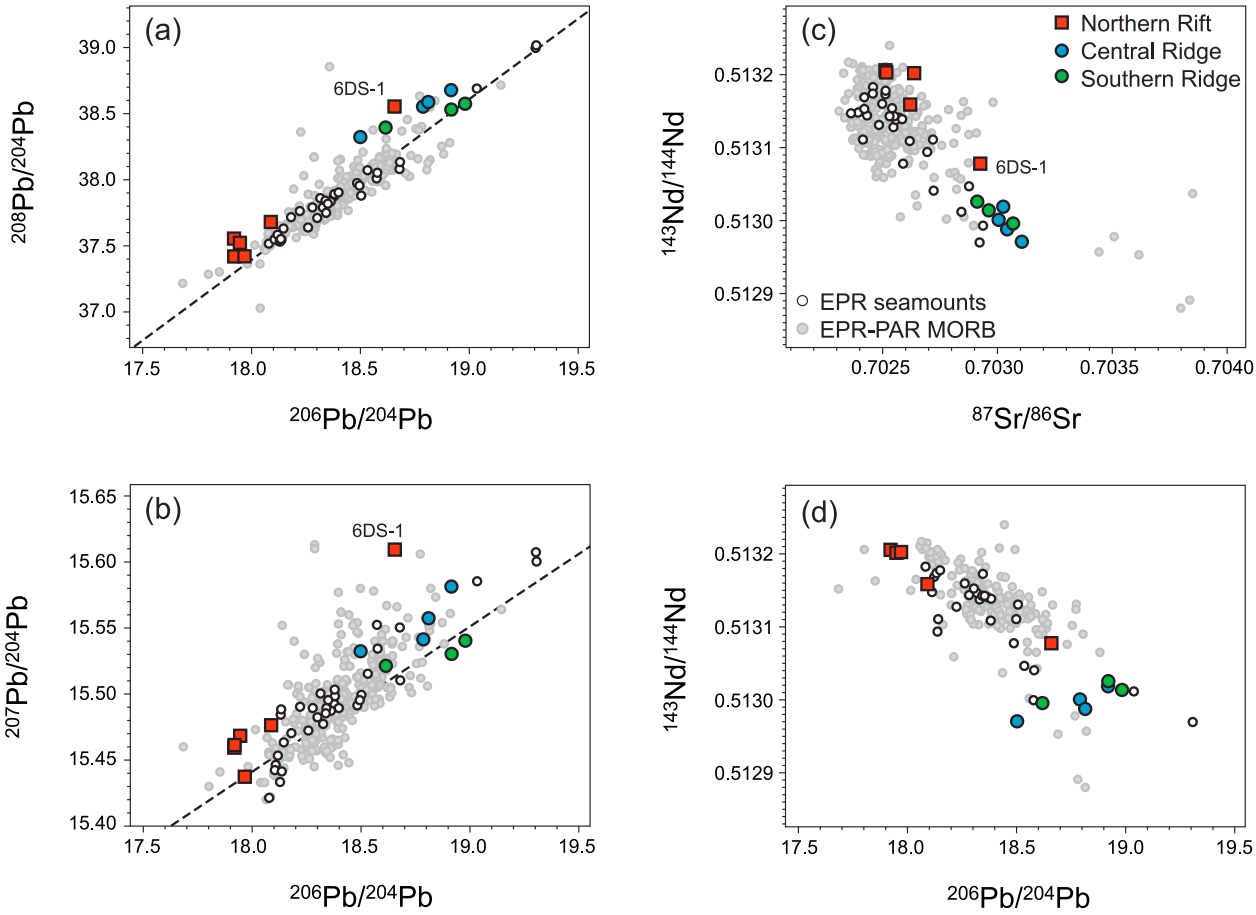


**Figure 5.** Radiogenic isotope compositions of lavas from the Galapagos Rise, with data for MORB from the East Pacific Rise and East Pacific Rise (PetDB database) and Pacific near-ridge seamounts [*Niu et al.*, 2002] shown for comparison. Galapagos Rise lavas cover most of the range in Sr, Nd, and Pb isotope compositions found in Pacific MORB. Excluding sample 6DS-1, postspreading lavas from the Central and Southern ridges have higher $^{87}Sr/^{86}Sr$, lower $^{143}Nd/^{144}Nd$ ratios, and more radiogenic Pb isotope compositions than older lavas from the Northern Rift that were erupted immediately before spreading ceased. (a and b) The dotted line is the Northern Hemisphere Reference Line [*Hart*, 1984].

of primitive MORB magmas are both sensitive to the degree of mantle melting [*Klein and Langmuir*, 1987; *Langmuir et al.*, 1992; *Niu and O'Hara*, 2008]; melts produced by smaller degrees of mantle melting have higher $Na_2O$, lower $SiO_2$ for a given MgO. Central and Southern Ridge lavas have higher $Na_{72}$ ($Na_2O$ concentrations corrected for the effects of low-pressure fractionation to Mg# = 72) and lower $Si_{72}$ values than the older Northern Rift lavas and most MORB from normal spreading centers (Figure 3). These differences can be explained if the younger, postspreading lavas result from smaller degrees of mantle melting. Significant changes in the average degree of mantle melting are expected during abandonment of a spreading ridge; the decreasing rate of mantle upwelling and the thickening lithosphere will both tend to result in a decrease in the average degree of melting with time. The changes in the thermal regime resulting from the slowdown of spreading on the dying Galapagos Rise therefore appear to have influenced both primary melt compositions and the subsequent fractional crystallization paths of these melts.

### 5.1.2. The Role of Mantle Heterogeneity

[26] To some extent, the variation observed in incompatible trace element ratios between lavas from the Northern Rift and from the Central and Southern ridges could also result from differences in the average degree and depth of melting. Qualitatively, smaller degrees of mantle melting at greater average pressure, with a greater proportion of melting occurring within the stability field of garnet peridotite, could account for the higher incompatible trace element concentrations, higher Nb/Zr,

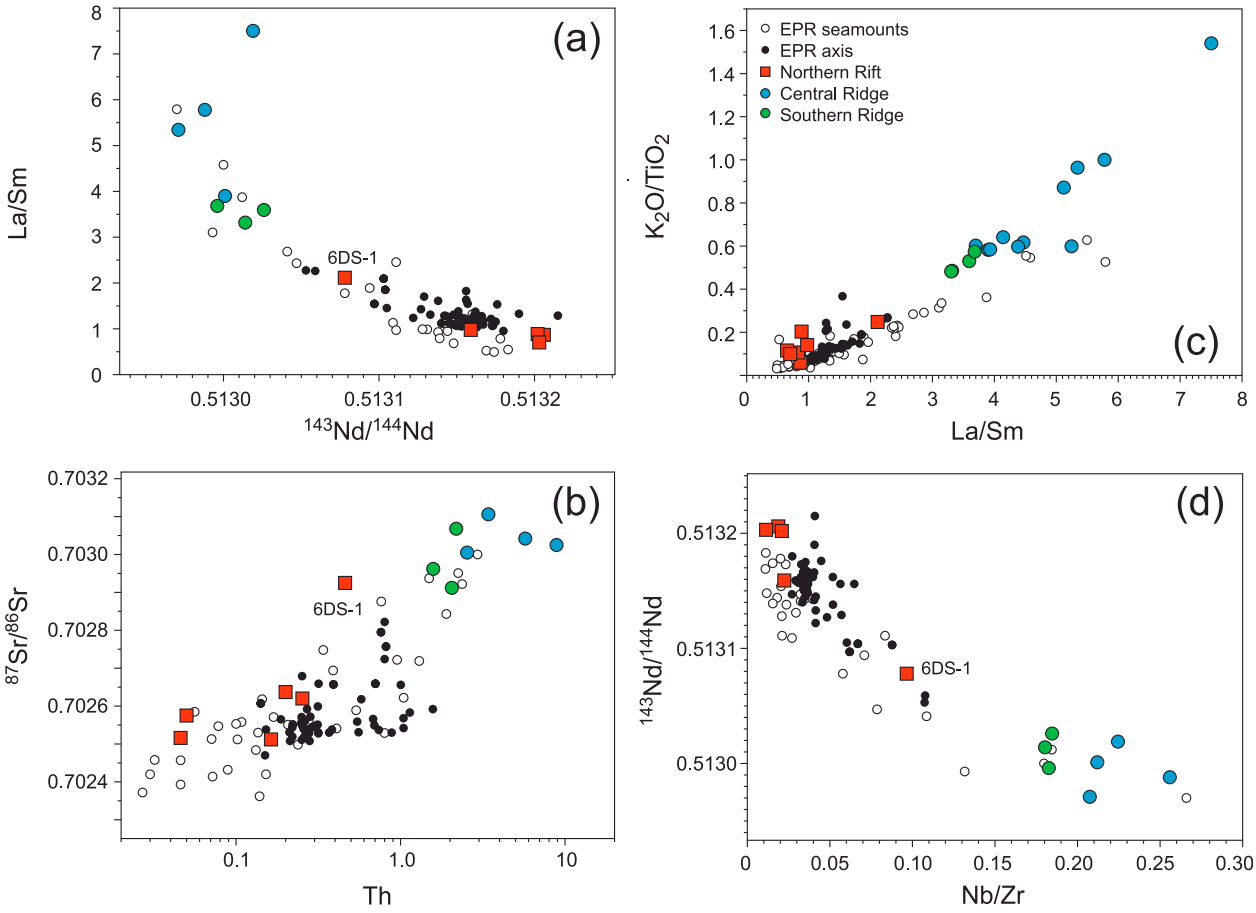


**Figure 6.** Trace element and isotope compositions of lavas from the Galapagos Rise. The large, correlated variations in incompatible element concentrations, incompatible element ratios, and isotope ratios cannot be explained by variable degrees of melting of a homogenous mantle source. Data for lavas from the EPR and Pacific near-ridge seamounts are shown for comparison (data sources are the same as for Figure 4).

$K_2O/TiO_2$, La/Yb and lower Yb/Nd in postspreading lavas from the Central and Southern ridges, compared to the older lavas from the Northern Rift. However, the absolute range in concentration of highly incompatible trace elements (a factor of 100 for Th and Nb, Figure 4) and the large range in incompatible trace element ratios such as Nb/Zr, La/Sm and $K_2O/TiO_2$, cannot be explained by any reasonable range in the degree of melting of a homogenous mantle source. Instead, the correlations between incompatible trace element ratios and Sr, Nd isotope composition (Figure 5) suggest that much of the variation in the former results from source heterogeneity.

[27] The variably depleted-enriched compositions of MORB erupted on individual spreading ridge segments is often attributed to mixing of normal, relatively depleted upper mantle with more enriched materials [e.g., *Schilling et al.*, 1983; *Castillo et al.*, 2000]. However, simple mixing processes are unable to explain the compositional variation within lavas from the Galapagos Rise. Two-component mixing of melts derived from lithologically distinct enriched and depleted mantle lithologies will result in linear arrays in the La/Nd-Yb/Nd and La/Yb-Sm/Yb diagrams, whereas the Galapagos-EPR data define curved arrays (Figure 8). For the same reason, melting of a source composed of two different lithologies, which are mixed in variable proportions (mixing of sources) but which both melt to the same extent, also cannot explain the observations. Instead, variable degrees of melting of a two-component mantle in which different lithologies have different trace element and isotope compositions but also different melting behavior may best account for the chemical and isotopic variation within Galapagos Rise lavas, as discussed in more detail below.

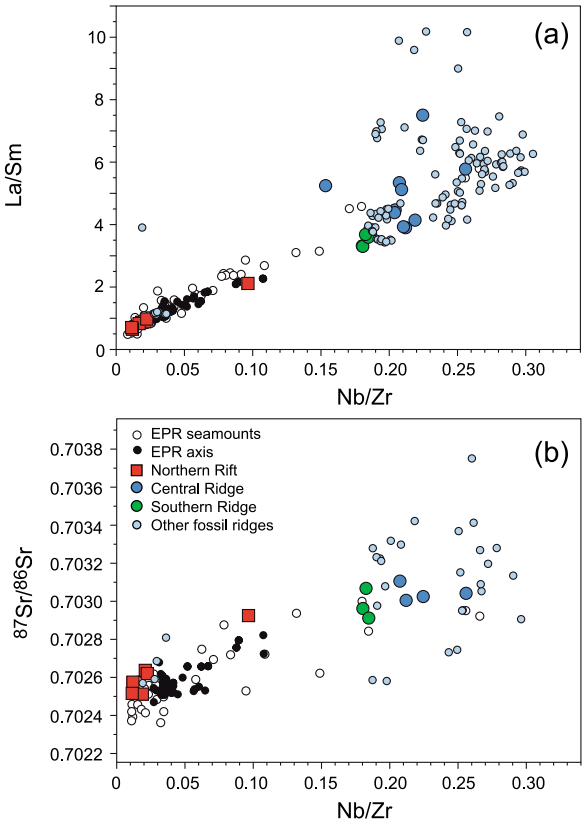


**Figure 7.** Comparison of trace element and isotope compositions of postspreading lavas from the Galapagos Rise (data from this study) with lavas from other fossil spreading centers worldwide (data from *Choe et al.* [2007], *Choi et al.* [2008], *Castillo et al.* [2010], and *Haase et al.* [2011]). Postspreading lavas include some of the most extreme EMORB compositions (high Nb/Zr, La/Sm, and $^{87}Sr/^{86}Sr$) found far from "hot spots." Data for lavas from the EPR and Pacific near-ridge seamounts are shown for comparison (data sources are the same as for Figure 4).

### 5.1.3. Melting of a Two-Component Mantle

[28] *Hirschmann and Stolper* [1996], *Phipps Morgan* [1999, 2001], *Ito and Mahoney* [2005a, 2005b], *Pearce* [2005], and *Stracke and Bourdon* [2009] have modeled quantitatively the effects of melting a mantle consisting of two or more chemically and isotopically distinct lithologies having different solidus temperature and melt productivity. As mantle upwells, these lithologies intersect their solidus temperatures at different times, and depending on their abundance and melt productivity, the more fertile components may become exhausted before reaching the top of the melting column. As they melt, more fertile lithologies extract heat from the surrounding more refractory lithologies, inhibiting melting of the latter; once more refractory lithologies do begin to melt, the remaining fertile materials may stop melting [*Phipps Morgan*, 2001]. A consequence of this behavior is that the resulting melting paths in figures such as Figures 8a–8d may be curved, kinked or discontinuous, as different lithologies begin to contribute to the instantaneous melt composition or become exhausted with increasing melt fraction. Another feature of such "melt extraction trajectories" [*Phipps Morgan*, 1999] is that because less than the total number of lithologies may undergo melting at any time, the range in composition of the melts produced with progressive melting is greater than would be the case if all lithologies contributed equally to the melt, although the pooled melts extracted from the melting column will generally have compositions that are intermediate between the end-member lithologies [*Phipps Morgan*, 1999; *Pearce*, 2005; *Stracke and Bourdon*, 2009]. In addition, *Ito and Mahoney* [2005a, 2005b] have shown that differences in the mantle flow field within the melting region have a significant influence on the relative amount of melt that is extracted from enriched and depleted lithologies.

[29] As discussed above, the major and trace element compositions of Galapagos Rise lavas together with the new $^{40}Ar$-$^{39}Ar$ ages indicate that the youngest lavas result from smaller degrees of mantle melting. During abandonment of a spreading ridge, the average degree of mantle melting is in fact expected to progressively decrease with time as the mantle upwelling rate slows and the overlying lithosphere thickens by conductive cooling [*Choe et al.*, 2007; *Choi et al.*, 2008]. Lavas produced by lower degrees of melting of heterogeneous mantle will contain a larger contribution from more fertile lithologies which are expected to have higher incompatible element concentrations, higher $^{87}Sr/^{86}Sr$ and lower $^{143}Nd/^{144}Nd$ [e.g., *Pearce*, 2005; *Stracke and Bourdon*, 2009]. We have therefore used a forward modeling approach and the melting equations of *Stracke and Bourdon* [2009] in order to examine whether variable degrees of melting of heterogeneous mantle can reproduce to first order the trace element and isotope variations within the Galapagos Rise lavas. We assume the simplest case of a two-component mantle, consisting of a volumetrically minor, incompatible element enriched component with high concentration of incompatible trace elements, high La/Yb and Nd/Yb, and higher

$^{87}Sr/^{86}Sr$, lower $^{143}Nd/^{144}Nd$ which has a lower solidus temperature and melt productivity than the surrounding more refractory lithology. We examine the range of melt compositions produced during variable degrees of melting of this source material using the melting model of *Stracke and Bourdon* [2009].

[30] The results are shown in Figure 8. Although the combination of model parameters we have used to calculate the melt extraction paths in Figure 8 are nonunique, the results of the modeling do show that variable degrees of melting of a two-component mantle can explain many aspects of the geochemistry of Galapagos Rise lavas. In particular, such models can reproduce the large variations in the ratios of highly incompatible elements, and the correlated variations in incompatible trace element and isotope ratios, which cannot be explained by melting of a homogenous mantle source. At progressively smaller degrees of melting, fertile enriched materials increasingly dominate melt compositions, and the resulting melt evolution trajectories can reproduce the curved data arrays defined by Galapagos Rise lavas in Figure 8. A similar temporal evolution of lava chemistry is observed in postspreading lavas from the extinct Phoenix Ridge in the Drake Passage [*Choe et al.*, 2007; *Choi et al.*, 2008; *Haase et al.*, 2011], and the fossil spreading centers off Baja California Sur [*Tian et al.*, 2011]. The chemical and isotopic evolution of postspreading lavas from fossil ridges may therefore represent some of the strongest evidence that the normal mantle beneath spreading ridges is highly heterogeneous on a length scale that is small relative to the size of the melting region. At actively spreading ridges, the average degree of melting is greater and melts are more efficiently mixed on their way to the surface, with the result that the composition of lavas erupted at active spreading ridges will provide a less accurate record of the degree of mantle heterogeneity. Nevertheless, the effects of source heterogeneity must be taken into account when using MORB to infer the composition of the mantle, as discussed in section 5.3.

[31] The highly variable Galapagos Rise lavas were erupted within a period of about 3.5 Myr, over a distance of 150 km, confirming the view that the upper mantle away from hot spots is highly heterogeneous. Thus at least on fossil ridges, large seamounts composed of EMORB can apparently be produced by small degrees of melting of normal upper mantle, in the absence of any nearby hot spot or plume.

## 5.2. Mantle Upwelling and Melting Beneath Spreading Ridges

[32] Lavas from fossil ridges provide an opportunity to examine the processes of mantle melting during slowdown of spreading and in the absence of plate separation and can potentially give insights into the nature of mantle upwelling beneath actively spreading ridges. The degree to which mantle upwelling beneath mid-ocean ridges is "active" rather than merely a passive response to plate separation has been extensively debated. Passive upwelling of mantle is an expected consequence of plate separation [*Spiegelman and McKenzie*, 1987; *Phipps Morgan et al.*, 1987], and the wide melt-containing zone beneath the EPR identified during the MELT experiment is consistent with upwelling driven by plate separation [*The Melt Seismic Team*, 1998]. However, some degree of active upwelling is predicted to result from "melting-induced buoyancy," due to thermal expansion and the presence of a melt phase and less dense residual peridotite [*Sotin and Parmentier*, 1989; *Parmentier and Phipps Morgan*, 1990]. It has also been proposed that variable, active mantle upwelling beneath mid-ocean ridges augments the passive upwelling and is responsible for ridge segmentation, with more active deep upwelling and greater melt production beneath ridge segment centers [*Macdonald et al.*, 1988; *Buck and Su*, 1989; *Scott and Stevenson*, 1989; *Lin et al.*, 1990].

[33] On most fossil ridges, the transition from normal spreading to no spreading apparently took place within about 1 Myr [*Batiza*, 1989), whereas postspreading magmatism occurs over timescales of 2–9 Myr after spreading ceased [*Batiza and Vanko*, 1985; *Batiza*, 1989; *Bohrson and Reid*, 1995; *Choe et al.*, 2007; *Clague et al.*, 2009; *Haase et al.*, 2011; this study]. Once formed, melt is efficiently extracted from the mantle within $10^3$–$10^5$ years [e.g., *Stracke et al.*, 2006], and so the age range of postspreading lavas requires a process that can actively generate melt over a period of up to 9 Myr after spreading ends. *Castillo et al.* [2010] proposed that beneath the thickening oceanic lithosphere at a fossil spreading center, melting in the absence of plate separation may result from (1) residual mantle upwelling due to the combined buoyancy effects of thermal expansion, melt depletion, and the presence of small melt fractions, or (2) melting of fertile lithologies as the thinner lithosphere at the fossil ridge drifts over previously undepleted mantle. At a fossil ridge, conductive cooling will erase significant differences in lithosphere thickness over a period of several tens of Myr after spreading

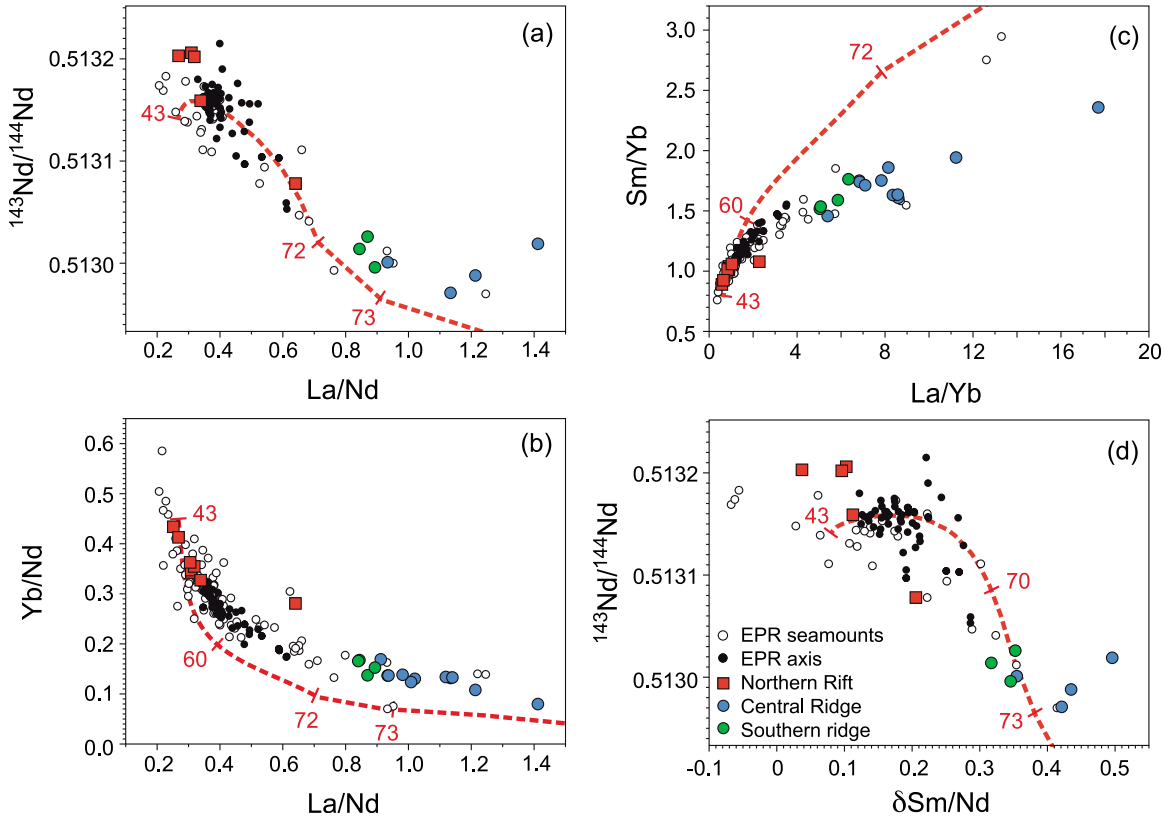


**Figure 8.** Variation of (a) Yb/Nd and (b) $^{143}Nd/^{144}Nd$ with La/Nd and $^{143}Nd/^{144}Nd$ with (c) Yb/Nd and (d) $\delta$Sm/Nd for Galapagos Rise lavas. The $\delta$Sm/Nd is defined as $\delta Sm/Nd = ((Sm/Nd)_{2Gyr} - (Sm/Nd)_m)/(Sm/Nd)_{2Gyr}$, where $(Sm/Nd)_{2Gyr}$ is the calculated source Sm/Nd based on the measured present-day $^{143}Nd/^{144}Nd$ ratio of the sample and assuming a 2Gyr mantle model age, and $(Sm/Nd)_m$ is the measured Sm/Nd ratio [*Salters*, 1996]. Two-component mixing of melts or sources result in linear arrays on these diagrams; the curved arrays defined by the Galapagos Rise lavas in Figures 8a–8c therefore cannot be explained by simple mixing of melts or by melting of two-component mantle in which enriched and depleted lithologies are mixed in variable proportions but contribute equally to melting. The negative correlation of $^{143}Nd/^{144}Nd$ with $\delta$Sm/Nd is unexpected if $\delta$Sm/Nd values are controlled only by the proportion of melting within the stability field of garnet. Instead, the trace element and isotope variations in Galapagos Rise lavas can be reproduced by variable degrees of melting of a mantle source consisting of different lithologies which melt at different rates. Curves show range in pooled melt compositions produced by variable degrees of fractional melting (residual porosity 0.1%) of a two-component mantle source, calculated using the method of *Stracke and Bourdon* [2009]. In this model, the source mantle contains "veins" of a volumetrically minor lithology ("pyroxenite"), which has higher incompatible trace element concentrations and higher La/Yb and Sm/Yb and lower Yb/Nd and $^{143}Nd/^{144}Nd$ than the enclosing peridotite matrix. The pyroxenite has a lower solidus temperature and therefore contributes more to melting at low melt fractions, compared to the more refractory matrix, which begins melting at a slightly lower pressure. In Figures 8a–8d, the resulting melt evolution paths are curved because with increasing degree of melting, the contribution to the pooled melt from the more fertile component with high incompatible trace element concentrations and high La/Nd and low Yb/Nd and $^{143}Nd/^{144}Nd$ progressively decreases. Melting functions, source mineralogy, and partition coefficients are taken from *Stracke and Bourdon* [2009]; numbers on the melting curves in Figures 8a–8d indicate the depth to the top of the melting column. Given the number of variables in these melting models, we have not attempted to adjust these parameters so as to perfectly reproduce the Galapagos Rise data set; rather the purpose of the modeling is to show that in contrast to binary mixing of end-member melt compositions, melting of heterogeneous mantle can produce curved arrays on these diagrams. Data for lavas from the EPR and Pacific near-ridge seamounts are shown for comparison (data sources are the same as for Figure 4).

ceases. If postspreading magmatism results from upwelling due to variations in lithosphere thickness, magmatism might be expected to continue over similar timescales. The observed age range of postspreading magmatism on fossil ridges is therefore consistent with melting resulting from mantle upwelling due to variations in lithosphere thickness. However, if lithosphere thickness con-

trols the location of postspreading magmatism, melting would be expected to occur preferentially at transform offsets, where differences in lithosphere thickness are most pronounced, and where upwelling resulting from movement of the lithosphere over the upper mantle would be concentrated. *Batiza* [1989] stated "…at the Mathematician and Guadelupe failed rifts, abundant postabandonment alkalic volcanism is found at failed rift-transform intersections…," but this does not appear to be the case along the Galapagos Rise [*Eakins and Lonsdale*, 2003], nor along sections of other fossil ridges which have been mapped in detail. It is possible that *Batiza and Vanko* [1985] may have mislocated the ridge axis along several of these fossil spreading centers due to the limited bathymetric data available at that time [*Tian et al.*, 2011]. More recent studies have shown that there is apparently a tendency for postspreading magmatism to construct axial seamounts away from segment ends [*Choe et al.*, 2007; *Haase et al.*, 2011; *Tian et al.*, 2011]. On the Galapagos Rise, bathymetric, magnetic and altimetric data show that elongate seamounts are present along much of the fossil ridge axis, with smaller, isolated seamounts nearer to segment ends and close to transforms [*Eakins and Lonsdale*, 2003]. There is no evidence for significant postspreading magmatism on the ridge segments immediately north or south of the large-offset South Gallego Fracture Zone, where young, thin lithosphere is juxtaposed against much older, thicker lithosphere.

[34] On the Galapagos Rise, the discontinuous distribution of postspreading magmatism, and its apparent concentration at the former ridge axis and closer to segment centers is more consistent with an origin from active mantle upwelling, either resulting from a component of active 3-D mantle flow or driven by the buoyancy of melt-depleted residual mantle beneath the ridge. In the latter case, the volume and duration of postspreading magmatism might be related to the degree of prior melt depletion. *Haase et al.* [2011] observed a possible correlation between the volume of postspreading volcanoes on fossil ridges and the former spreading rate of the ridge. If the degree of mantle melting beneath spreading ridges is related to spreading rate [*Niu and Hekinian*, 1997], such a correlation may indicate that melting-induced buoyancy is important. On the other hand, the duration of postspreading magmatism at fossil ridges (up to 8 Myr on Davidson Seamount [*Clague et al.*, 2009]) may be longer than can be accounted for by density contrasts resulting from prior melting, and indicate that a component of active, 3-D upwelling is responsible for continued magmatism on fossil ridges. The distribution and age range of postspreading lavas on fossil ridges therefore suggest that active upwelling contributes to the passive mantle upwelling beneath actively spreading ridges, especially close to segment centers. The lack of significant postspreading volcanism on the Northern Rift may result from less intense upwelling close to the major South Gallego Fracture Zone, or from less fertile mantle beneath this ridge segment, as also proposed to explain the discontinuous distribution of postspreading volcanism along fossil spreading centers elsewhere [*Castillo et al.*, 2010].

## 5.3. Implications for Chemical and Isotopic Variation in Global MORB

[35] We have shown that the range in incompatible trace element ratios such as La/Yb, Nb/Zr and $K_2O/TiO_2$ in Galapagos Rise lavas is dominantly the result of variations in the degree of melting of a heterogeneous mantle. In this location, the effects of source heterogeneity are relatively large, due to the decreasing degrees of melting resulting from slowdown and cessation of spreading. Similarly heterogeneous mantle likely underlies much of the global spreading system, as indicated by the similarity of postspreading lavas on fossil ridges worldwide (Figure 7), and highly variable lavas erupted on seamounts on the flanks of spreading ridges [*Batiza and Vanko*, 1984; *Zindler et al.*, 1984; *Niu and Batiza*, 1997; *Niu et al.*, 2002]. The larger degrees of mantle melting and more complete magma mixing effects beneath active spreading ridges result in less chemical and isotopic variation within MORB erupted at active ridges. However, variations in the degree of melting resulting from differences in the degree of upwelling or mantle temperature, or variations in the relative volumes and compositions of enriched and depleted lithologies could exert an influence on MORB chemistry both within individual ridge segments and between different sections of ridge. As a result, it may not be straightforward to infer the average depth and degree of melting beneath mid-ocean ridges based on the trace element variation within MORB.

[36] Nevertheless, numerous studies have attempted to estimate the approximate depth and degree of mantle melting beneath spreading ridges from the trace element compositions of MORB. For example, *Salters* [1996] found that MORB erupted on deeper sections of the MOR system tend to have a stronger garnet signal as inferred from the difference between Lu/Hf and Sm/Nd ratios of MORB and time-

integrated source ratios inferred from $^{176}Hf/^{177}Hf$ and $^{143}Nd/^{144}Nd$. This observation apparently conflicts with the major element systematics of MORB, which have been interpreted to indicate that beneath shallow ridge segments the mantle is hotter and begins melting deeper, so that a greater proportion of the melt is generated within the stability field of garnet [*Klein and Langmuir*, 1987; *Langmuir et al.*, 1992]. *Salters* [1996] therefore proposed that beneath deeper ridges the melting region is broader at its base, such that a greater proportion of melting occurs within the stability field of garnet. In contrast, beneath shallow ridges the melting region is inferred to extend to greater depths, but because it is columnar in shape a smaller proportion of the total melt is generated within the stability field of garnet [*Salters*, 1996]. In contrast, *Shen and Forsyth* [1995] argued that the variation in the apparent garnet signature is predominantly due to variations in the final depth (uppermost limit) of melting, which lies at greater depth beneath deeper ridge segments. A deeper final depth of melting could result from higher conductive cooling to the surface, or a lesser degree of mantle upwelling. Both parameters are expected to be affected by spreading rate, but there is no simple relationship between spreading rate and ridge depth. Another explanation for the Sm/Yb depth relationship [*Shen and Forsyth*, 1995] is that deeper ridges are underlain by more fertile, garnet-rich mantle, which upwells more slowly due to its higher density, thus causing melting to cease at a greater depth [*Niu and O'Hara*, 2008]. In this model, the melts produced at deep ridges have higher Sm/Yb because they are less diluted by melts of more refractory peridotite with low Sm/Yb [*Niu and O'Hara*, 2008].

[37] Our new data for young postspreading lavas from the Galapagos Rise show that variations in the extent of melting of normal heterogeneous mantle have a very significant effect on the La/Yb, Sm/Nd ratios (and hence inferred garnet effect) of lavas erupted in this location. *Salters* [1996] and *Shen and Forsyth* [1995] attempted to correct for the effects of mantle heterogeneity on the REE compositions of MORB, but our results suggest that this may not always be successful. For example, *Salters* [1996] calculated $\delta$Sm/Nd values for MORB, a measure of the difference between the measured Sm/Nd ratio in a lava and the time-integrated source Sm/Nd ratio inferred from Nd isotope compositions, and these $\delta$Sm/Nd values were assumed to be related to the magnitude of the garnet effect during melting. However, $\delta$Sm/Nd values of Galapagos Rise lavas are correlated negatively with $^{143}Nd/^{144}Nd$ ratios (Figure 8), a relationship which is not expected if variations in $\delta$Sm/Nd result only from the proportion of melting within the stability field of garnet. The compositional range of the Galapagos Rise lavas is similar to that of lavas from near-ridge seamounts on the flanks of the EPR, suggesting that a similarly heterogeneous mantle is widespread beneath the Pacific far from hot spots. The correlations of $\delta$Sm/Nd and Sm/Yb with $Na_{8.0}$, $Na_{72}$ and axial depth for spreading ridges worldwide [*Salters*, 1996; *Shen and Forsyth*, 1995] may therefore result from variations in either the average degree of melting of heterogeneous mantle, or the relative proportions of enriched to depleted lithologies, rather than the depth of melting relative to the spinel-garnet peridotite transition. Beneath deep ridges the average degree of melting is smaller, and/or the mantle is more enriched, so that a fertile component with high Sm/Yb contributes more to the total melt [*Niu and O'Hara*, 2008]. Lower degrees of melting at greater average depth beneath deep ridges could result from a lower degree of mantle upwelling [*Shen and Forsyth*, 1995; *Niu and O'Hara*, 2008], or possibly from greater loss of heat to the surface due to hydrothermal circulation, which is predicted to penetrate to greater depths at deep ridges due to the higher hydrostatic pressure [*Kasting et al.*, 2006].

[38] If more enriched mantle lithologies preferentially contribute to melting beneath active spreading ridges, then the isotopic composition of MORB will not faithfully record that of the upper mantle, as is commonly assumed. Instead, MORB compositions may be biased toward more radiogenic Sr, Pb and Os, and less radiogenic Nd and Hf compositions [e.g., *Phipps Morgan*, 1999; *Stracke and Bourdon*, 2009], and a complementary "hidden" depleted component will be retained in the melting residues. The $^{143}Nd/^{144}Nd$ ratios of clinopyroxenes from abyssal peridotites extend to higher values than associated MORB [*Snow et al.*, 1994; *Salters and Dick*, 2002; *Cipriani et al.*, 2004; *Warren et al.*, 2009] and Os isotope compositions of abyssal peridotites are less radiogenic than those of MORB [*Harvey et al.*, 2006; *Liu et al.*, 2008]; accurate Hf and Pb isotope data for abyssal peridotites are needed to confirm this effect.

## 6. Summary and Conclusions

[39] We used major and trace element and Sr, Nd and Pb isotope data, together with $^{39}Ar$-$^{40}Ar$ ages for lavas from the Galapagos Rise in the eastern Pacific, to investigate the evolution in magma

compositions erupted during slowdown and after the end of active spreading on this fossil mid-ocean ridge. Magmatism on the Galapagos Rise continued for at least 2 Myr after active spreading ceased, and younger postspreading lavas are more alkalic, have higher concentrations of incompatible elements, higher La/Yb, K/Ti, $^{87}Sr/^{86}Sr$, and lower $^{143}Nd/^{144}Nd$ ratios than lavas inferred to have erupted immediately before spreading ended. The very large range in trace element and isotope compositions cannot be explained by melting of a homogenous mantle source, or by two-component mixing of enriched and depleted end-member melts, or by melting of variably enriched mantle in which both enriched and depleted lithologies contribute equally to melting. Instead, the trace element and isotope variations can be produced by variable degrees of melting of a two-component mantle in which incompatible trace element enriched lithologies with lower melting temperature preferentially contribute to the melt at low degrees of melting. Postspreading lavas from the Galapagos Rise therefore contain a greater contribution from enriched mantle lithologies with lower Sm/Nd and $^{143}Nd/^{144}Nd$, which yield melts with higher $\delta$Sm/Nd, and do not necessarily require a greater proportion of melting in the stability field of garnet peridotite. Our results, combined with those from other fossil spreading centers and seamounts on the flanks of spreading ridges, provide clear evidence for a significant influence of variable degrees of melting of heterogeneous mantle on the chemical variation in lavas erupted at spreading ridges away from hot spots. This effect must be taken into account when using the compositions of MORB to infer the conditions of melting beneath active spreading ridges. We suggest that the correlations between ridge depth and $\delta$Sm/Nd, Sm/Yb and fractionation-corrected Na concentrations in lavas for actively spreading ridges worldwide may result from variations in mantle fertility and/or variations in the average degree of melting, rather than large variations in mantle temperature. If more enriched mantle lithologies with low $^{143}Nd/^{144}Nd$, high $^{87}Sr/^{86}Sr$ are preferentially melted during mantle upwelling beneath active spreading ridges, then the upper mantle may have significantly higher $^{143}Nd/^{144}Nd$, lower $^{87}Sr/^{86}Sr$ and a less radiogenic Pb isotope composition than is commonly inferred from analyses of MORB.

## Acknowledgments

[40] We are grateful to Captain Andresen and his crew for their help during *Sonne* cruise SO160 and to D. Garbe-Schönberg, C. Voigt, F. Hauff, and B. Mader for helping with the analytical work. G. Ito and A. Stracke very kindly provided us with copies of their mantle melting models and advised us on their use. We thank C. Beier and A. Stracke for useful discussions and the two journal reviewers for their helpful comments. This study was funded by the Bundesministerium für Bildung und Forschung through grant 03G0160A.

## References

Anderson, R. N., and J. G. Sclater (1972), Topography and evolution of the East Pacific Rise between 5°S and 20°S, *Earth Planet. Sci. Lett.*, *14*, 433–441, doi:10.1016/0012-821X(72)90145-8.

Arevalo, R., and W. F. McDonough (2010), Chemical variations and regional diversity observed in MORB, *Chem. Geol.*, *271*, 70–85, doi:10.1016/j.chemgeo.2009.12.013.

Batiza, R. (1977), Petrology and chemistry of Guadalupe Island: An alkalic seamount on a fossil ridge crest, *Geology*, *5*, 760–764, doi:10.1130/0091-7613(1977)5<760:PACOGI>2.0.CO;2.

Batiza, R. (1989), Failed rifts, in *The Geology of North America*, vol. N, *The Eastern Pacific Ocean and Hawaii*, edited by E. L. Winterer, D. M. Hussong, and R. W. Decker, pp. 177–186, Geol. Soc. of Am., Boulder, Colo.

Batiza, R., and C. G. Chase (1981), Miocene spreading centre south of Isla Guadelupa, *Nature*, *289*, 787–789, doi:10.1038/289787a0.

Batiza, R., and D. Vanko (1984), Petrology of young Pacific seamounts, *J. Geophys. Res.*, *89*, 11,235–11,260, doi:10.1029/JB089iB13p11235.

Batiza, R., and D. A. Vanko (1985), Petrologic evolution of large failed rifts in the eastern Pacific: Petrology of volcanic and plutonic rocks from the Mathematician Ridge area and the Guadelupe Trough, *J. Petrol.*, *26*, 564–602.

Batiza, R., R. Oestrike, and K. Futa (1982), Chemical and isotopic diversity in basalts dredged from the East Pacific Rise at 10°S, the fossil Galapagos Rise and the Nazca Plate, *Mar. Geol.*, *49*, 115–132, doi:10.1016/0025-3227(82)90032-9.

Bohrson, W. A., and M. R. Reid (1995), Petrogenesis of alkaline basalts from Socorro Island, Mexico: Trace element evidence for contamination of ocean island basalt in the shallow ocean crust, *J. Geophys. Res.*, *100*, 24,555–24,576, doi:10.1029/95JB01483.

Buck, W. R., and W. Su (1989), Focused mantle upwelling below mid-ocean ridges due to feedback between viscosity and melting, *Geophys. Res. Lett.*, *16*, 641–644, doi:10.1029/GL016i007p00641.

Castillo, P. R., E. Klein, J. Bender, C. Langmuir, R. Batiza, and W. White (2000), Petrology and Sr, Nd, and Pb isotope geochemistry of mid-ocean ridge basalt glasses from the 11°45′N to 15°00′N segment of the East Pacific Rise, *Geochem. Geophys. Geosyst.*, *1*(11), 1011, doi:10.1029/1999GC000024.

Castillo, P. R., D. A. Clague, A. S. Davis, and P. F. Lonsdale (2010), Petrogenesis of Davidson Seamount lavas and its implications for fossil spreading center and intraplate magmatism in the eastern Pacific, *Geochem. Geophys. Geosyst.*, *11*, Q02005, doi:10.1029/2009GC002992.

Choe, W. H., J. I. Lee, M. J. Lee, S. D. Hur, and Y. K. Jin (2007), Origin of E-MORB in a fossil spreading center: The Antarctic-Phoenix Ridge, Drake Passage, Antarctica, *Geosci. J.*, *11*, 185–199, doi:10.1007/BF02913932.

Choi, S. H., W. H. Choe, and J. I. Lee (2008), Mantle heterogeneity beneath the Antarctic-Phoenix Ridge off Antarctic Peninsula, *Isl. Arc*, *17*, 172–182, doi:10.1111/j.1440-1738.2007.00609.x.

Cipriani, A., H. K. Brueckner, E. Bonatti, and D. Brunelli (2004), Oceanic crust generated by elusive parents: Sr and Nd isotopes in basalt-peridotite pairs from the Mid-Atlantic Ridge, *Geology*, *32*, 657–660, doi:10.1130/G20560.1.

Clague, D. A., J. B. Paduan, R. A. Duncan, J. J. Huard, A. S. Davis, P. R. Castillo, P. Lonsdale, and A. DeVoelaere (2009), Five million years of compositionally diverse, episodic volcanism: Construction of Davidson Seamount atop an abandoned spreading center, *Geochem. Geophys. Geosyst.*, *10*, Q12009, doi:10.1029/2009GC002665.

Davis, A. S., S. H. Gunn, W. A. Bohrson, L.-B. Gray, and J. R. Hein (1995), Chemically diverse, sporadic volcanism at seamounts offshore southern and Baja California, *Geol. Soc. Am. Bull.*, *107*, 554–570, doi:10.1130/0016-7606(1995)107<0554:CDSVAS>2.3.CO;2.

Davis, A. S., D. A. Clague, W. A. Bohrson, G. B. Dalrymple, and H. G. Greene (2002), Seamounts at the continental margin of California: A different kind of oceanic intraplate volcanism, *Geol. Soc. Am. Bull.*, *114*, 316–333, doi:10.1130/0016-7606(2002)114<0316:SATCMO>2.0.CO;2.

Donnelly, K. E., S. L. Goldstein, C. H. Langmuir, and M. Spiegelman (2004), Origin of enriched ocean ridge basalts and implications for mantle dynamics, *Earth Planet. Sci. Lett.*, *226*, 347–366, doi:10.1016/j.epsl.2004.07.019.

Duncan, R. A., and R. A. Keller (2004), Radiometric ages for basement rocks from the Emperor Seamounts, ODP Leg 197, *Geochem. Geophys. Geosyst.*, *5*, Q08L03, doi:10.1029/2004GC000704.

Eakins, B. W., and P. Lonsdale (2003), Structural patterns and tectonic history of the Bauer microplate, Eastern Tropical Pacific, *Mar. Geophys. Res.*, *24*, 171–205, doi:10.1007/s11001-004-5882-4.

Eason, D., and J. Sinton (2006), Origin of high-Al N-MORB by fractional crystallisation in the upper mantle beneath the Galapagos Spreading Center, *Earth Planet. Sci. Lett.*, *252*, 423–436, doi:10.1016/j.epsl.2006.09.048.

Garbe-Schönberg, C.-D. (1993), Simulataneous determination of thirty-seven trace elements in twenty-eight international rock standards by ICP-MS, *Geostand. Newsl.*, *17*, 81–97, doi:10.1111/j.1751-908X.1993.tb00122.x.

Haase, K. M. (1996), The relationship between the age of the lithosphere and the composition of oceanic magmas: Constraints on partial melting, mantle sources and the thermal structure of the plates, *Earth Planet. Sci. Lett.*, *144*, 75–92, doi:10.1016/0012-821X(96)00145-8.

Haase, K. M., et al. (2002), GARIMAG-Magmatism at the fossil spreading axis of the Galapagos Rise, SE Pacific, *Cruise Rept. SO-160*, Inst. für Geowiss., Univ. Kiel, Kiel, Germany.

Haase, K. M., C. Beier, S. Fretzdorff, P. T. Leat, R. A. Livermore, T. L. Barry, J. A. Pearce, and F. Hauff (2011), Magmatic evolution of a dying spreading axis: Evidence for the interaction of tectonics and mantle heterogeneity from the fossil Phoenix Ridge, Drake Passage, *Chem. Geol.*, *280*, 115–125, doi:10.1016/j.chemgeo.2010.11.002.

Hart, S. R. (1984), A large-scale isotope anomaly in the Southern Hemisphere mantle, *Nature*, *309*, 753–757, doi:10.1038/309753a0.

Harvey, J., A. Gannoun, K. W. Burton, N. W. Rogers, O. Alard, and I. J. Parkinson (2006), Ancient melt extraction from the oceanic upper mantle revealed by Re-Os isotopes in abyssal peridotites from the Mid-Atlantic Ridge, *Earth Planet. Sci. Lett.*, *244*, 606–621, doi:10.1016/j.epsl.2006. 02.031.

Hébert, H., B. Villemant, C. Deplus, and M. Diament (1999), Contrasting geophysical and geochemical signatures of a volcano at the axis of the Wharton fossil ridge (N-E Indian Ocean), *Geophys. Res. Lett.*, *26*, 1053–1056, doi:10.1029/1999GL900160.

Herron, E. M. (1972), Sea-floor spreading and the Cenozoic history of the East-Central Pacific, *Geol. Soc. Am. Bull.*, *83*, 1671–1692, doi:10.1130/0016-7606(1972)83[1671:SSATCH]2.0.CO;2.

Hirano, N., et al. (2006), Volcanism in response to plate flexure, *Science*, *313*, 1426–1428, doi:10.1126/science.1128235.

Hirschmann, M. M., and E. M. Stolper (1996), A possible role for garnet pyroxenite in the origin of the 'garnet signature' in MORB, *Contrib. Mineral. Petrol.*, *124*, 185–208, doi:10.1007/s004100050184.

Hoernle, K., and G. Tilton (1991), Sr-Nd-Pb isotope data for Fuerteventura (Canary Islands) basal complex and subaerial volcanics: Application to magma genesis and evolution, *Schweiz. Mineral. Petrogr. Mitt.*, *71*, 3–18.

Ito, G., and J. J. Mahoney (2005a), Flow and melting of a heterogeneous mantle: 1. Method and importance to the geochemistry of ocean island and mid-ocean ridge basalts, *Earth Planet. Sci. Lett.*, *230*, 29–46, doi:10.1016/j.epsl.2004.10.035.

Ito, G., and J. J. Mahoney (2005b), Flow and melting of a heterogeneous mantle: 2. Implications for a chemically nonlayered mantle, *Earth Planet. Sci. Lett.*, *230*, 47–63, doi:10.1016/j.epsl.2004.10.034.

Janney, P. E., J. D. Macdougall, J. H. Natland, and M. A. Lynch (2000), Geochemical evidence from the Pukapuka volcanic ridge system for a shallow enriched mantle domain beneath the South Pacific Superswell, *Earth Planet. Sci. Lett.*, *181*, 47–60, doi:10.1016/S0012-821X(00)00181-3.

Kasting, J. F., M. T. Howard, K. Wallmann, J. Veizer, G. Shields, and J. Jaffres (2006), Paleoclimates, ocean depth, and the oxygen isotopic composition of seawater, *Earth Planet. Sci. Lett.*, *252*, 82–93, doi:10.1016/j.epsl.2006. 09.029.

Klein, E. M., and C. H. Langmuir (1987), Global correlations of oceanic ridge basalt chemistry with axial depth and crustal thickness, *J. Geophys. Res.*, *92*, 8089–8115, doi:10.1029/JB092iB08p08089.

Konter, J., H. Staudigel, J. Blichert-Toft, B. B. Hanan, M. Polve, G. R. Davies, N. Shimizu, and P. Schiffman (2009), Geochemical stages at Jasper Seamount and the origin of intraplate volcanoes, *Geochem. Geophys. Geosyst.*, *10*, Q02001, doi:10.1029/2008GC002236.

Koppers, A. A. P. (2002), ArArCALC—Software for $^{40}Ar/^{39}Ar$ age calculations, *Comput. Geosci.*, *28*, 605–619, doi:10.1016/S0098-3004(01)00095-4.

Koppers, A. A. P., H. Staudigel, and R. A. Duncan (2003), High-resolution $^{40}Ar/^{39}Ar$ dating of the oldest oceanic basement basalts in the western Pacific basin, *Geochem. Geophys. Geosyst.*, *4*(11), 8914, doi:10.1029/2003GC000574.

Langmuir, C. H., E. M. Klein, and T. Plank (1992), Petrological systematics of mid-ocean ridge basalts: Constraints on melt generation beneath ocean ridges, in *Mantle Flow and Melt Generation at Mid-Ocean Ridges*, *Geophys. Monogr. Ser.*, vol. 71, edited by J. Phipps Morgan, D. K. Blackman, and J. M. Sinton, pp. 183–280, AGU, Washington D. C.

Lin, J., G. M. Purdy, H. Schouten, J.-C. Sempere, and C. Zervas (1990), Evidence from gravity data for focused magmatic accretion along the Mid-Atlantic Ridge, *Nature*, *344*, 627–632, doi:10.1038/344627a0.

Liu, C.-Z., J. E. Snow, E. Hellebrand, G. Brügmann, A. von der Handt, A. Büchl, and A. W. Hofmann (2008), Ancient, highly heterogeneous mantle beneath Gakkel Ridge, Arctic Ocean, *Nature*, *452*, 311–316, doi:10.1038/nature06688.

Macdonald, K. C., P. J. Fox, L. J. Perram, M. F. Eisen, R. M. Haymon, S. P. Miller, S. M. Carbotte, M.-H. Cormier, and A. N. Shor (1988), A new view of the mid-ocean ridge from the behaviour of ridge-axis discontinuities, *Nature*, *335*, 217–225, doi:10.1038/335217a0.

Mammerickx, J., E. Herron, and L. Dorman (1980), Evidence for two fossil spreading ridges in the southwest Pacific, *Geol. Soc. Am. Bull.*, *91*, 263–271, doi:10.1130/0016-7606(1980)91<263:EFTFSR>2.0.CO;2.

McKenzie, D., and R. K. O'Nions (1991), Partial melt distributions from inversion of rare earth element concentrations, *J. Petrol.*, *32*, 1021–1091.

Menard, H. W., T. E. Chase, and S. M. Smith (1964), Galapagos Rise in the southeastern Pacific, *Deep Sea Res.*, *11*, 233–242.

Michael, P. J., and W. C. Cornell (1998), Influence of spreading rate and magma supply on crystallisation and assimilation beneath mid-ocean ridges: Evidence from chlorine and major element chemistry of mid-ocean ridge basalts, *J. Geophys. Res.*, *103*, 18,325–18,356, doi:10.1029/98JB00791.

Niu, Y., and R. Batiza (1997), Trace element evidence from seamounts for recycled oceanic crust in the eastern Pacific mantle, *Earth Planet. Sci. Lett.*, *148*, 471–483, doi:10.1016/S0012-821X(97)00048-4.

Niu, Y., and R. Hekinian (1997), Spreading-rate dependence of the extent of mantle melting beneath ocean ridges, *Nature*, *385*, 326–329, doi:10.1038/385326a0.

Niu, Y., and M. J. O'Hara (2008), Global correlations of ocean ridge basalt chemistry with axial depth: A new perspective, *J. Petrol.*, *49*, 633–664, doi:10.1093/petrology/egm051.

Niu, Y., K. D. Collerson, R. Batiza, J. I. Wendt, and M. Regelous (1999), Origin of enriched-type mid-ocean ridge basalt at ridges far from mantle plumes: The East Pacific Rise at 11°20′N, *J. Geophys. Res.*, *104*, 7067–7087, doi:10.1029/1998JB900037.

Niu, Y., M. Regelous, J. I. Wendt, R. Batiza, and M. J. O'Hara (2002), Geochemistry of near-EPR seamounts: Importance of source vs. process and the origin of enriched mantle component, *Earth Planet. Sci. Lett.*, *199*, 327–345, doi:10.1016/S0012-821X(02)00591-5.

Parmentier, E. M., and J. Phipps Morgan (1990), The spreading rate dependence of three-dimensional spreading centre structure, *Nature*, *348*, 325–328, doi:10.1038/348325a0.

Pearce, J. A. (2005), Mantle preconditioning by melt extraction during flow: Theory and petrogenetic implications, *J. Petrol.*, *46*, 973–997, doi:10.1093/petrology/egi007.

Phipps Morgan, J. (1999), Isotope topology of individual hotspot basalt arrays: Mixing curves or melt extraction trajectories?, *Geochem. Geophys. Geosyst.*, *1*, 1003, doi:10.1029/1999GC000004.

Phipps Morgan, J. (2001), Thermodynamics of pressure release melting of a veined plum pudding mantle, *Geochem. Geophys. Geosyst.*, *2*, 1001, doi:10.1029/2000GC000049.

Phipps Morgan, J., E. M. Parmentier, and J. Lin (1987), Mechanisms for the origin of mid-ocean ridge axial topography: Implications for the thermal and mechanical structure of accretion plate boundaries, *J. Geophys. Res.*, *92*, 12,823–12,836, doi:10.1029/JB092iB12p12823.

Pilet, S., J. Hernandez, P. Sylvester, and M. Poujol (2005), The metasomatic alternative for ocean island basalt chemical heterogeneity, *Earth Planet. Sci. Lett.*, *236*, 148–166, doi:10.1016/j.epsl.2005.05.004.

Presnall, D. C., J. R. Dixon, T. H. O'Donnell, and S. A. Dixon (1979), Generation of mid-ocean ridge tholeiites, *J. Petrol.*, *20*, 3–35.

Prinzhofer, A., E. Lewin, and C. J. Allegre (1989), Stochastic melting of the marble cake mantle: Evidence from local study of the East Pacific Rise at 12°50′ N, *Earth Planet. Sci. Lett.*, *92*, 189–206, doi:10.1016/0012-821X(89)90046-0.

Regelous, M., Y. Niu, J. I. Wendt, R. Batiza, A. Greig, and K. D. Collerson (1999), Variations in the geochemistry of magmatism on the East Pacific Rise at 10°30′N since 880 ka, *Earth Planet. Sci. Lett.*, *168*, 45–63, doi:10.1016/S0012-821X(99)00048-5.

Regelous, M., A. W. Hofmann, W. Abouchami, and S. J. G. Galer (2003), Geochemistry of lavas from the Emperor Seamounts, and the geochemical evolution of Hawaiian magmatism from 85 to 42 Ma, *J. Petrol.*, *44*, 113–140, doi:10.1093/petrology/44.1.113.

Salters, V. J. M. (1996), The generation of mid-ocean ridge basalts from the Hf and Nd isotope perspective, *Earth Planet. Sci. Lett.*, *141*, 109–123, doi:10.1016/0012-821X(96)00070-2.

Salters, V. J. M., and H. J. B. Dick (2002), Mineralogy of the mid-ocean ridge basalt source from neodymium isotopic compositions of abyssal peridotites, *Nature*, *418*, 68–72, doi:10.1038/nature00798.

Salters, V. J. M., and S. R. Hart (1989), The hafnium paradox and the role of garnet in the source of mid-ocean-ridge basalts, *Nature*, *342*, 420–422, doi:10.1038/342420a0.

Schilling, J. G., M. Zajac, R. Evans, T. Johnston, W. White, J. D. Devine, and R. Kingsley (1983), Petrologic and geochemical variations along the Mid-Atlantic Ridge from 29°N to 73°N, *Am. J. Sci.*, *283*, 510–586, doi:10.2475/ajs.283.6.510.

Scott, D. R., and D. J. Stevenson (1989), A self-consistent model of melting, magma migration and buoyancy-driven circulation beneath mid-ocean ridges, *J. Geophys. Res.*, *94*, 2973–2988, doi:10.1029/JB094iB03p02973.

Shen, Y., and D. W. Forsyth (1995), Geochemical constraints on initial and final depth of melting beneath mid-ocean ridges, *J. Geophys. Res.*, *100*, 2211–2237, doi:10.1029/94JB02768.

Sleep, N. H. (1984), Tapping of magmas from ubiquitous mantle heterogeneities: An alternative to mantle plumes?, *J. Geophys. Res.*, *89*, 10,029–10,041, doi:10.1029/JB089iB12p10029.

Snow, J. E., S. R. Hart, and H. J. B. Dick (1994), Nd and Sr isotope evidence linking mid-ocean ridge basalts and abyssal peridotites, *Nature*, *371*, 57–60, doi:10.1038/371057a0.

Sotin, C. J., and E. M. Parmentier (1989), Dynamical consequences of compositional and thermal density stratification beneath spreading centers, *Geophys. Res. Lett.*, *16*, 835–838, doi:10.1029/GL016i008p00835.

Spiegelman, M., and T. Elliott (1993), Consequences of melt transport for uranium series disequilibrium in young lavas, *Earth Planet. Sci. Lett.*, *118*, 1–20, doi:10.1016/0012-821X(93)90155-3.

Spiegelman, M., and D. P. McKenzie (1987), Simple 2-D models for melt extraction at mid-ocean ridges and island arcs, *Earth Planet. Sci. Lett.*, *83*, 137–152, doi:10.1016/0012-821X(87)90057-4.

Stracke, A., and B. Bourdon (2009), The importance of melt extraction for tracing mantle heterogeneity, *Geochim. Cosmochim. Acta*, *73*, 218–238, doi:10.1016/j.gca.2008.10.015.

Stracke, A., B. Bourdon, and D. P. McKenzie (2006), Melt extraction in the Earth's mantle: Constraints from U-Th-Pa-Ra studies in oceanic basalts, *Earth Planet. Sci. Lett.*, *244*, 97–112, doi:10.1016/j.epsl.2006.01.057.

The MELT Seismic Team (1998), Imaging the deep seismic structure beneath a mid-ocean ridge: The MELT Experiment, *Science*, *280*, 1215–1218, doi:10.1126/science.280.5367.1215.

Tian, L., P. R. Castillo, P. F. Lonsdale, D. Hahm, and D. R. Hilton (2011), Petrology and Sr-Nd-Pb-He isotope geochemistry of postspreading lavas on fossil spreading axes off Baja California Sur, Mexico, *Geochem. Geophys. Geosyst.*, *12*, Q0AC10, doi:10.1029/2010GC003319.

Todt, W., R. A. Cliff, A. Hanser, and A. W. Hofmann (1996), Evaluation of a $^{202}$Pb-$^{205}$Pb double spike for high-precision lead isotope analysis, in *Earth Processes: Reading the Isotopic Code*, *Geophys. Monogr. Ser.*, vol. 95, edited by A. Basu and S. Hart, pp. 429–437, AGU, Washington, D. C.

Tormey, D. R., T. L. Grove, and W. B. Bryan (1987), Experimental petrology of normal MORB near the Kane Fracture Zone: 22°–25°N, Mid-Atlantic Ridge, *Contrib. Mineral. Petrol.*, *96*, 121–139, doi:10.1007/BF00375227.

Warren, J. M., N. Shimizu, C. Sakaguchi, H. J. B. Dick, and E. Nakamura (2009), An assessment of upper mantle heterogeneity based on abyssal peridotite isotopic compositions, *J. Geophys. Res.*, *114*, B12203, doi:10.1029/2008JB006186.

Wendt, J. I., M. Regelous, Y. Niu, R. Hekinian, and K. D. Collerson (1999), Geochemistry of lavas from the Garrett Transform Fault: Insights into mantle heterogeneity beneath the eastern Pacific, *Earth Planet. Sci. Lett.*, *173*, 271–284, doi:10.1016/S0012-821X(99)00236-8.

Zindler, A., H. Staudigel, and R. Batiza (1984), Isotope and trace element geochemistry of young Pacific seamounts: Implications for the scale of upper mantle heterogeneity, *Earth Planet. Sci. Lett.*, *70*, 175–195, doi:10.1016/0012-821X(84)90004-9.